

## ABSTRACT

Title of thesis: COMPUTATIONAL STUDIES  
OF DROPLET MOTION AND DEFORMATION  
IN A MICROFLUIDIC CHANNEL WITH A CONSTRICTION

Moon Soo Lee, Master of Science, 2010

Thesis directed by: Professor Panagiotis Dimitrakopoulos  
Department of Chemical Engineering

In the present thesis, we investigate the interfacial dynamics of a three-dimensional droplet in a viscous fluid flowing through a square microfluidic channel with a rectangular cross-sectional constriction. The effects of various parameters of the two fluids and the sizes of the constriction geometry are considered. The numerical computation for the current problem requires a highly-accurate and efficient method owing to the very small/large deformation of the droplet shape at low/high flow rates, the small droplet-solid gap and the complicated three-dimensional geometries. An efficient fully-implicit three-dimensional Spectral Boundary Element method developed by Dimitrakopoulos [11] is employed.

Our results show that the droplet dynamics is significantly influenced by the non-symmetric shape of the rectangular cross-sectional constriction, i.e. owing to the constriction shape the droplet deforms much less in the flow-direction by forming a flat disk shape. As the capillary number is decreased, the droplet deformation in the flow-direction decreases owing to the larger surface tension. The effects of the viscosity ratio are complicated with viscosity ratio near unity showing the largest deformation.

COMPUTATIONAL STUDIES OF DROPLET MOTION AND DEFORMATION  
IN A MICROFLUIDIC CHANNEL WITH A CONSTRICTION

by

Moon Soo Lee

Thesis submitted to the Faculty of the Graduate School of the  
University of Maryland, College Park in partial fulfillment  
of the requirements for the degree of  
Master of Science  
2010

Advisory Committee:

Professor Panagiotis Dimitrakopoulos, Chair/Advisor  
Professor Richard V Calabrese  
Professor Kyu Yong Choi  
Professor Sheryl H. Ehrman

© Copyright by  
Moon Soo Lee  
2010

## Acknowledgements

I would like to thank all the people who have made this thesis possible.

First of all, I would like to thank my advisor, Professor Panagiotis Dimitrakopoulos, for his guidance and support in my research during my master's program and for his tremendous help in my thesis preparation.

I thank all the members of our research lab, Mrs. Shugi Kuriakose and Mr. Kishore Mamidi, for their helpful discussions.

I am also thankful to the staff of the Chemical Engineering Department for their kind assistance.

I own my gratitude to my parents, Mr. Cheolwon Lee and Mrs. Hyeja Kim, for their love and prayer.

This research was supported in part by the Petroleum Research Fund of the American Chemical Society and the National Center for Supercomputing Applications in Illinois.

# Table of Contents

List of Tables	v
List of Figures	vi
1 Introduction	1
1.1 Objectives of the Current Study . . . . .	2
1.2 Literature Survey on the Droplet Squeezing through a Constriction . . . . .	3
1.3 Literature Survey on Numerical Methods . . . . .	6
1.4 Overview of Current Research . . . . .	7
2 Mathematical Formulation	10
2.1 Derivation of Boundary Integral Equations(BIE) . . . . .	10
2.2 BIE for a Droplet in a Channel . . . . .	12
2.3 Dimensionless Parameters of the Current Problem . . . . .	13
2.4 Rest Physical Variables of Interest . . . . .	15
3 Numerical Method for Interfacial Dynamics	16
3.1 Spectral Element Formulation . . . . .	16
3.2 Explicit Time-integration Algorithm . . . . .	17
3.3 Implicit Time-integration Algorithm . . . . .	19
3.4 Spectral Boundary Element Discretization of a Droplet in a Channel . . . . .	20
4 Results and Discussion	22
4.1 Validation . . . . .	22

4.2	Rectangular and Square Constriction . . . . .	24
4.3	Rectangular Constriction . . . . .	33
4.3.1	Effects of Capillary Number . . . . .	33
4.3.2	Effects of Viscosity Ratio . . . . .	43
4.3.3	Effects of Constriction Length . . . . .	52
4.3.4	Effects of Constriction Gap . . . . .	60
4.4	Conclusion . . . . .	69
	Bibliography	71

## List of Tables

3.1	Diagonally-implicit Runge-Kutta (DIRK) scheme of third order [11]	. 19
-----	---	------

## List of Figures

1.1	Illustration of a droplet in a square channel with a rectangular constriction. . . . .	8
1.2	Illustration of the constriction having different lengths and minimum gap. . . . .	9
2.1	Illustrations for the geometry of the BIEs (2.3) and (2.15). . . . .	11
2.2	Illustration of a droplet in the fluid inside a channel with constriction.	13
3.1	Spectral Boundary Element discretization of a channel and a droplet.	21
4.1	Validation of our algorithm by comparison with previous studies: (a),(b),(c) from Tsai and Miksis [45] and (d) from Martinez and Udell [28]. The solid dots represent our data. . . . .	23
4.2	Perspective of square channels with (a) a rectangular and (b) a square full-cosine constriction of 1.0 length and 1.0 minimum gap. . . . .	26
4.3	(a) Droplet centroid $X_c$ versus time $t$ and (b) droplet velocity $U_x$ versus its centroid $X_c$ for a droplet with $a = 0.6$ , $Ca = 0.1$ and $\lambda = 5$ squeezing through a rectangular and a square full-cosine constriction with 1.0 length and 1.0 minimum gap. . . . .	27
4.4	Evolution of the droplet profile with $Ca = 0.1$ , $\lambda = 5$ , $a = 0.6$ , at $t = 0, 1, 1.25, 1.5, 1.75, 2.0, 3$ squeezing through a rectangular and a square full-cosine constriction with 1.0 length and 1.0 minimum gap ( $y$ -axis view). . . . .	28

4.5	Three-dimensional $y$ and $z$ -axis shapes of the droplets with $a = 0.6$ , $Ca = 0.1$ , $\lambda = 5$ , at $X_c = -0.5, 0, 0.5$ , squeezing through a rectangular and a square full-cosine constriction with 1.0 length and 1.0 minimum gap. . . . .	30
4.6	(a) Droplet $x$ -length $L_x$ and (b) $y$ -length $L_y$ versus its centroid $X_c$ for a droplet with $a = 0.6$ , $Ca = 0.1$ and $\lambda = 5$ squeezing through a rectangular and a square full-cosine constriction with 1.0 length and 1.0 minimum gap. . . . .	31
4.7	Droplet $z$ -length $L_z$ versus its centroid $X_c$ for a droplet with $a = 0.6$ , $Ca = 0.1$ and $\lambda = 5$ squeezing through a rectangular and a square full-cosine constriction with 1.0 length and 1.0 minimum gap. . . . .	32
4.8	(a) Droplet surface area $S_d$ and (b) droplet-solid minimum distance $h_{min}$ versus its centroid $X_c$ for a droplet with $a = 0.6$ , $Ca = 0.1$ and $\lambda = 5$ squeezing through a rectangular and a square full-cosine constriction with 1.0 length and 1.0 minimum gap. . . . .	34
4.9	Three-dimensional $y$ and $z$ -axis shapes of the droplets with $a = 0.6$ , $Ca = 0.05, 0.1, 0.2$ , $\lambda = 5$ , at $X_c = 0$ , squeezing through a rectangular full-cosine constriction with 1.0 length and 1.0 minimum gap. . . . .	37
4.10	(a) Droplet centroid $X_c$ versus time $t$ and (b) droplet velocity $U_x$ versus its centroid $X_c$ for a droplet with $a = 0.6$ , $Ca = 0.05, 0.1$ and $0.2$ and $\lambda = 5$ squeezing through a rectangular full-cosine constriction with 1.0 length and 1.0 minimum gap. . . . .	38

4.11 (a) Droplet $x$ -length $L_x$ and (b) $y$ -length $L_y$ versus its centroid $X_c$ for a droplet with $a = 0.6$ , $Ca = 0.05, 0.1$ and $0.2$ and $\lambda = 5$ squeezing through a rectangular full-cosine constriction with $1.0$ length and $1.0$ minimum gap. . . . .	39
4.12 Droplet $z$ -length $L_z$ versus its centroid $X_c$ for a droplet with $a = 0.6$ , $Ca = 0.05, 0.1$ and $0.2$ and $\lambda = 5$ squeezing through a rectangular full-cosine constriction with $1.0$ length and $1.0$ minimum gap. . . . .	40
4.13 (a) Droplet surface area $S_d$ and (b) droplet-solid minimum distance $h_{min}$ versus its centroid $X_c$ for a droplet with $a = 0.6$ , $Ca = 0.05, 0.1$ and $0.2$ and $\lambda = 5$ squeezing through a rectangular full-cosine constriction with $1.0$ length and $1.0$ minimum gap. . . . .	41
4.14 Minimum distance between the droplet and the solid $h_{min} = 0.031$ at $X_c = 0.47$ for a droplet with $a = 0.6$ , $Ca = 0.05$ and $\lambda = 5$ squeezing through a rectangular full-cosine constriction with $1.0$ length and $1.0$ minimum gap. . . . .	42
4.15 Three-dimensional shape of a droplet with $a = 0.6$ , $Ca = 0.2$ , $\lambda = 5$ forming a dimple at the rear-part of the droplet at its centroid $X_c = 1.3$ (heart-shape). . . . .	43
4.16 Three-dimensional $y$ and $z$ -axis shapes of the droplets with $a = 0.6$ , $Ca = 0.1$ , $\lambda = 0, 1, 10$ , at $X_c = 0$ , squeezing through a rectangular full-cosine constriction with $1.0$ length and $1.0$ minimum gap. . . . .	47

4.17 (a) Droplet centroid $X_c$ versus time $t$ and (b) droplet velocity $U_x$ versus its centroid $X_c$ for a droplet with $a = 0.6$ , $Ca = 0.1$ and $\lambda = 0, 0.1, 1, 5$ and 10 squeezing through a rectangular full-cosine constriction with 1.0 length and 1.0 minimum gap. . . . .	48
4.18 (a) Droplet $x$ -length $L_x$ and (b) $y$ -length $L_y$ versus its centroid $X_c$ for a droplet with $a = 0.6$ , $Ca = 0.1$ and $\lambda = 0, 0.1, 1, 5$ and 10 squeezing through a rectangular full-cosine constriction with 1.0 length and 1.0 minimum gap. . . . .	49
4.19 Droplet $z$ -length $L_z$ versus its centroid $X_c$ for a droplet with $a = 0.6$ , $Ca = 0.1$ and $\lambda = 0, 0.1, 1, 5$ and 10 squeezing through a rectangular full-cosine constriction with 1.0 length and 1.0 minimum gap. . . . .	50
4.20 (a) Droplet surface area $S_d$ and (b) droplet-solid minimum distance $h_{min}$ versus its centroid $X_c$ for a droplet with $a = 0.6$ , $Ca = 0.1$ and $\lambda = 0, 0.1, 1, 5$ and 10 squeezing through a rectangular full-cosine constriction with 1.0 length and 1.0 minimum gap. . . . .	51
4.21 Minimum distance between the droplet and the solid $h_{min} = 0.027$ at $X_c = 0.46$ for a droplet with $a = 0.6$ , $Ca = 0.05$ and $\lambda = 10$ squeezing through a rectangular full-cosine constriction with 1.0 length and 1.0 minimum gap. . . . .	54
4.22 Geometries of square channels with a rectangular full-cosine constriction having 1.0, 2.0, 3.0 length and 1.0 minimum gap. . . . .	55

4.23	Three-dimensional shapes of the droplets with $a = 0.6$ , $Ca = 0.1$ , $\lambda = 5$ , at $X_c = 0$ , squeezing through a rectangular full-cosine constriction with 1.0, 2.0, 3.0 length and 1.0 minimum gap. . . . .	56
4.24	(a) Droplet centroid $X_c$ versus time $t$ and (b) droplet velocity $U_x$ versus its centroid $X_c$ for a droplet with $a = 0.6$ , $Ca = 0.1$ and $\lambda = 5$ squeezing through a rectangular full-cosine constriction with 1.0, 2.0, 3.0 length and 1.0 minimum gap. . . . .	57
4.25	(a) Droplet $x$ -length $L_x$ and (b) $y$ -length $L_y$ versus its centroid $X_c$ for a droplet with $a = 0.6$ , $Ca = 0.1$ and $\lambda = 5$ squeezing through a rectangular full-cosine constriction with 1.0, 2.0, 3.0 length and 1.0 minimum gap. . . . .	58
4.26	Droplet $z$ -length $L_z$ versus its centroid $X_c$ for a droplet with $a = 0.6$ , $Ca = 0.1$ and $\lambda = 5$ squeezing through a rectangular full-cosine constriction with 1.0, 2.0, 3.0 length and 1.0 minimum gap. . . . .	59
4.27	(a) Droplet surface area $S_d$ and (b) droplet-solid minimum distance $h_{min}$ versus its centroid $X_c$ for a droplet with $a = 0.6$ , $Ca = 0.1$ and $\lambda = 5$ squeezing through a rectangular full-cosine constriction with 1.0, 2.0, 3.0 length and 1.0 minimum gap. . . . .	61
4.28	Geometries of square channels with a rectangular full-cosine constriction having 1.0 length and 1.4, 1.0 minimum gap. . . . .	62
4.29	Three-dimensional shapes of the droplets with $a = 0.6$ , $Ca = 0.1$ , $\lambda = 5$ , at $X_c = 0$ , squeezing through a rectangular full-cosine constriction with 1.0 length and 1.4, 1.0 minimum gap. . . . .	63

4.30 (a) Droplet centroid  $X_c$  versus time  $t$  and (b) droplet velocity  $U_x$  versus its centroid  $X_c$  for a droplet with  $a = 0.6$ ,  $Ca = 0.1$  and  $\lambda = 5$  squeezing through a rectangular full-cosine constriction with 1.0 length and 1.4, 1.0 minimum gap. . . . . 64

4.31 (a) Droplet  $x$ -length  $L_x$  and (b)  $y$ -length  $L_y$  versus its centroid  $X_c$  for a droplet with  $a = 0.6$ ,  $Ca = 0.1$  and  $\lambda = 5$  squeezing through a rectangular full-cosine constriction with 1.0 length and 1.4, 1.0 minimum gap. . . . . 65

4.32 Droplet  $z$ -length  $L_z$  versus its centroid  $X_c$  for a droplet with  $a = 0.6$ ,  $Ca = 0.1$  and  $\lambda = 5$  squeezing through a rectangular full-cosine constriction with 1.0 length and 1.4, 1.0 minimum gap. . . . . 66

4.33 (a) Droplet surface area  $S_d$  and (b) droplet-solid minimum distance  $h_{min}$  versus its centroid  $X_c$  for a droplet with  $a = 0.6$ ,  $Ca = 0.1$  and  $\lambda = 5$  squeezing through a rectangular full-cosine constriction with 1.0 length and 1.4, 1.0 minimum gap. . . . . 68

# Chapter 1

## Introduction

In the present thesis, we investigate the interfacial dynamics of a three-dimensional droplet in a viscous fluid flowing through a square channel with a rectangular cross-sectional constriction. The problem of a droplet squeezing through a constriction in a capillary channel is of fundamental importance as a prototype study that can be applicable to many industrial and physiological processes. We closely investigate the physics of the problem for a wide range of capillary number  $Ca$ , viscosity ratio  $\lambda$ , and geometric size of the channel and the constriction.

An efficient three-dimensional fully-implicit Spectral Boundary Element method developed by Dimitrakopoulos [11] is used to solve the problem. We emphasize that this is a challenging computational problem because it requires (i) a highly accurate stable numerical method due to the very small/large deformation of the droplet at low/high flow rates, and the close interaction between the droplet and the solid surfaces and (ii) an efficient algorithm for the large-size complicated three-dimensional geometries.

## 1.1 Objectives of the Current Study

The study of a droplet squeezing through a constricted capillary is a prototype model for the two-phase flow in porous media and microfluidic channels which can be found in many areas of research. It is encountered in many industrial processes (e.g. enhanced oil recovery, oil sand processing, ground water purification, fixed-bed catalytic reactors and microfluidic devices) and in physiological processes (e.g. red blood cell motion in blood vessels and *in vivo* transportation of drugs through tissues or capillary networks).

Previously, intense amount of studies has been motivated by its application to enhanced oil recovery as the oil price has rocketed over the past few decades [44]. The physics involved in the displacement of oil droplets through a pore constriction via injection of another fluid was the key to understanding and improving the efficiency of the oil recovery [31].

Recently, the ongoing development of advanced microfluidic devices has motivated further studies in this area. A flow-focusing device that can synthesize highly monodisperse droplets, bubbles and particles of controlled size has shown numerous potential applications [22, 43]. The ability to control the flow rate and the sequence of reagents addition with extreme precision has allowed new methods for biological and chemical reactions and analysis [38, 40].

We emphasize that a prototype study may embrace the challenge of scaling up in order to be closer to an application, especially for a large-scale study such as the oil recovery process. However, the fundamental understanding of the droplet

interfacial dynamics in a single channel helps much in the physical understanding of the large-scale complicated geometries.

## **1.2 Literature Survey on the Droplet Squeezing through a Constriction**

Many prototype models have been designed to study the dynamics of droplets in constricted capillary channels. The motion of droplets in a viscous fluid through a constriction has several parameters that determine the flow. These parameters include the geometry of the capillary pore, fluids properties and fluid-fluid interaction parameters. Depending on these factors, a droplet can either flow through the constriction, break up into daughter droplets or become trapped at the neck of the constriction. Due to this complexity, each individual study normally focuses on a specific phenomenon.

A plethora of literature has covered the droplet motion and the snap-off mechanism in viscous flows in a straight tube [2, 21, 28]. For a droplet moving through a constricted capillary tube, Roof studied the snap-off as a mechanism that traps oil drops in porous media [37]. He found a pressure equilibrium position of a meniscus of an oil-water interface beyond which the snap-off would occur. Numerous experimental studies were conducted to understand the behavior of droplet in constrictions [16, 51, 30, 19, 1]. Han and Funatsu [19] conducted experiments on the deformation and snap-off of droplets in converging tubes. Olbricht and Leal [30] performed experiments on a droplet moving through a circular tube varying in di-

ameter and reported the significance of the effect of geometry on the deformation and the snap-off of the droplet. Gauglitz, St. Laurent and Radke [16] experimentally studied the snap-off of large droplets in a constricted capillary channel and determined the breakup time and the produced droplet's length. Later they derived an evolution equation for the thickness of a thin film between the droplet and the wall in the constricted geometry and showed that the film grows in time and snaps off the droplet. Arriola and Willhite [1] conducted experiments on an oil droplet in a non-circular pore throat along with the effect of surfactants on the mobilization of the droplet. They found a region for stable and unstable droplet motion in terms of the effect of interfacial tension, flow velocity and droplet length. They also observed that due to the corners of the non-circular throat and thus the higher flow rate, the snap-off process is faster.

Along with the experimental studies, theoretical and numerical studies have also been conducted. Ratulowski and Chang [36] based on a linear stability analysis studied the snap-off at a strong constriction for both axisymmetric and square constriction. Martinez and Udell [27] numerically studied a droplet in periodically constricted tube but did not find snap-off or trapping. Tsai and Miksis [45] used an axisymmetric boundary integral method to study the droplet snap-off process and the effects of the capillary number, viscosity ratio and geometry sizes. Studies of capsules in capillary channels, where the thin membrane properties have to be considered, were also conducted. Leyrat-Maurin and Barthes-Biesel [26] studied the motion of a capsule through a hyperbolic constriction. For an overview of droplet motion in a tube or a channel mentioned above, Olbricht has presented a review

of the prototype studies of multi-phase flow in porous media [31]. Muradoglu and Gokaltun’s algorithm is based on the two-dimensional front-tracking method while they studied a freely-rising drop in a single constriction or a periodically constricted channels. The interactions of two buoyancy-driven drops in a continuously constricted channel were also investigated [29]. Later, the algorithm was extended to study buoyancy-driven motion and breakup of viscous drops in sinusoidally constricted channels with respect to the effects of the channel geometry, drop size and Bond number [32]. They reported critical values for the droplet break-up. Studies that are focused on the trapping of a droplet where reported. Most recently, Zinchenko and Davis [54, 4] studied a droplet squeezing through a granular model constriction using a boundary integral method utilizing a Heberker representation. They were able to obtain results for the condition of a droplet trapping at the pore neck of granular geometries. They also emphasized that the ability of an algorithm to determine the near-critical conditions for the trapping is highly challenging due to the small droplet-wall gap.

Another closely related prototype study for the current thesis is the study of droplet motion in a rectangular channel or between two infinite parallel planes. Rectangular microchannels resemble many of the microchannels in microfluidic devices [25, 3, 42]. The rectangular channels can give the advantages of high loadability and low sample dispersion at the same time [42]. Previous studies investigated the droplet motion confined between two infinite parallel plates. Shapris and Haber conducted a theoretical work to study the migration of a two-dimensional droplet in parallel planes [39]. Staben, Zinchenko & Davis studied a three-dimensional parti-

cle between parallel planes using a boundary integral method [41]. Vananroye *et al.* conducted an experimental study of a three-dimensional droplet under shear flow between parallel plates and showed the difference in the motion of the droplet compared to bulk flow [46, 47]. They reported the effect of the confined geometry on the droplet deformation, the critical capillary number and the critical viscosity of breaking. Griggs *et al.* studied the behavior of a three-dimensional single deformable drop in a Poiseuille flow between two infinite parallel plane walls by numerical computation. Aside from the relationships between deformation,  $Ca$  and wall proximity, they also focused on the three-dimensional droplet shape [18].

To our knowledge, the current thesis is the first numerical study of a droplet motion in a rectangular constriction. The interfacial dynamics of a droplet squeezing through a non-axisymmetric constriction differs from that in an axisymmetric constriction or in between two infinite parallel walls owing to the effects of the non-axisymmetric directions of expansion and compression of the droplet.

### 1.3 Literature Survey on Numerical Methods

There has been abundant application of the boundary integral method in the field of fluid dynamics for low-Reynolds number flows over the past three decades. The efficiency of the boundary integral method results from avoiding the calculation within the flow domain. Since Youngren and Acrivos [53] first introduced the method in the study of interfacial dynamics in Stokes flow, the versatility of the method has allowed the study of many different problems such as rigid particles, droplet

deformation and breakup, particle-wall interaction and deformation of red blood cells. Many versions of the boundary integral method has been developed based on different discretization schemes [45, 41, 54, 23].

Among them, the spectral boundary element method has been developed to utilize the high accuracy of the spectral method [6, 49, 11]. The main attraction of the spectral boundary element method is the exponential convergence in numerical accuracy while maintaining the versatility of the boundary element method. Dimitrakopoulos and Higdon has employed the spectral boundary element method in the study of a droplet displacement from a solid surface under Stokes flow [5, 6, 8] and gravitational force [7]. Later, Wang and Dimitrakopoulos studied the hemodynamic forces exerted on endothelial cells or leukocytes adhering to the surface of blood vessels [49, 48] and Dimitrakopoulos studied the deformation and the sliding of a droplet adhering to a solid surface in shear flow [10] and gravitational force [13]. Recently, Dodson and Dimitrakopoulos extended its application in studied a capsules in Stokes flow [14, 15].

## 1.4 Overview of Current Research

In this thesis, we study the dynamics of a droplet squeezing through a rectangular cross-sectional constriction under constant flow rate and no-slip boundary conditions in low-Reynolds number flows as shown in Figure 1.1.

The mathematical formulation and the numerical method are discussed in Chapter 2 and 3, respectively. In Chapter 4, a general case model is studied first

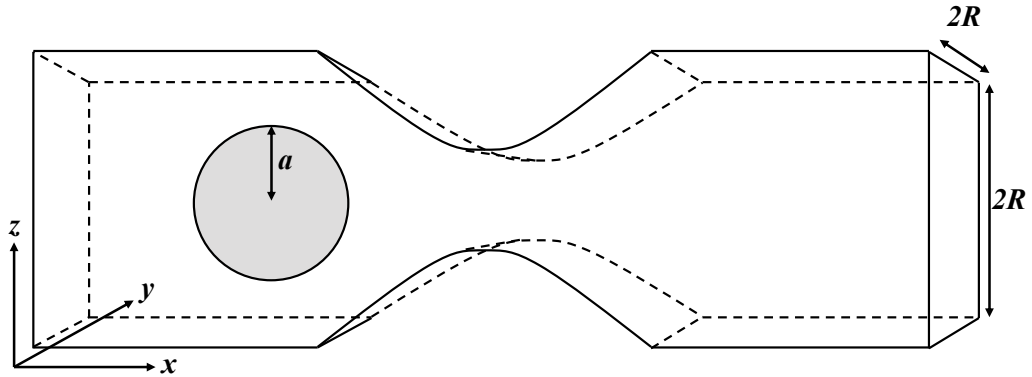


Figure 1.1: Illustration of a droplet in a square channel with a rectangular constriction.

and then various comparison cases are examined to see the effects of the physical and geometrical parameters.

For all computations, both fluids are considered isothermal and Newtonian while the surface tension is constant and the gravitational effects are neglected. We restrict the half-length of the square cross-section of the channel to  $R = 1$  and droplet size to  $a = 0.6$  initially placed before the constriction so that the center of mass of the droplet is located at  $X_c = -3$ . We determine the droplet velocity  $U_x$ , droplet length, width and height  $L_x, L_y, L_z$ , droplet surface area  $S_d$  and minimum distance  $h_{min}$  between the droplet and solid wall with respect to time  $t$  and the droplet center of mass  $X_c$ .

The parameters affecting the problem include the size of the constriction,

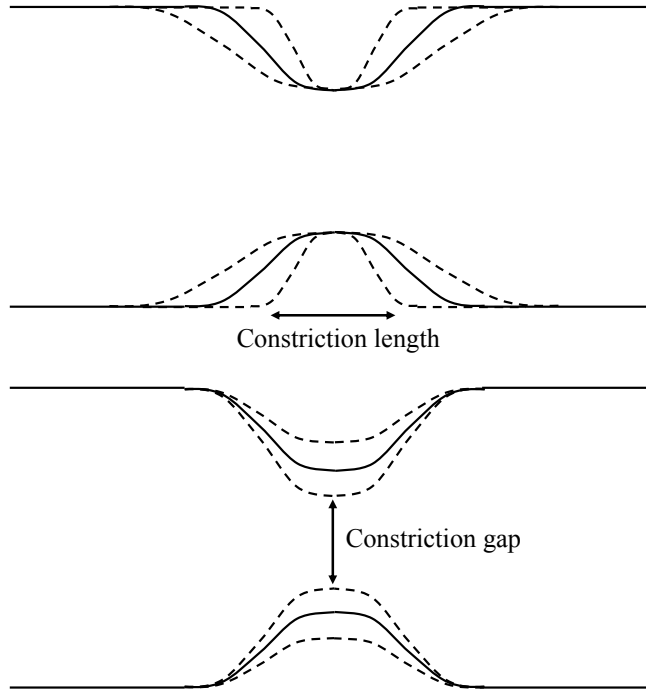


Figure 1.2: Illustration of the constriction having different lengths and minimum gap.

capillary number  $Ca$  and viscosity ratio  $\lambda$ . Figure 1.2 illustrates geometries of different the constriction length and minimum gap sizes we investigate.

The equation for our full-cosine constriction is

$$z = R - 0.5d[1.0 + \cos(\pi x/l)] \quad (1.1)$$

where  $R$  is the half-length of the side of the channel and  $d$  is the constriction depth.

$x$  varies  $-l \leq x \leq l$  so that equation (1.1) represents full cosine bump.

## Chapter 2

# Mathematical Formulation

### 2.1 Derivation of Boundary Integral Equations(BIE)

When the Reynolds number is sufficiently small, the inertial terms in the Navier-Stokes equations are neglected and the flow is governed by the Stokes equations

$$\nabla \cdot \boldsymbol{\sigma} \equiv -\nabla p + \mu \nabla^2 \mathbf{u} = 0 \quad (2.1)$$

and the continuity equation

$$\nabla \cdot \mathbf{u} = 0 \quad (2.2)$$

where  $\boldsymbol{\sigma}$  represents the stress tensor,  $p$  is the dynamic pressure,  $\mu$  is the viscosity of the fluid and  $\mathbf{u}$  is the velocity vector.

By introducing the fundamental solutions  $S_{ij}$  and  $T_{ijk}$  for the three-dimensional Stokes equations (2.1) and the continuity equation (2.2), and then integrating over a volume of fluid bounded by a surface  $S_B$  shown in Figure 2.1(a), the velocity at a point  $\mathbf{x}_0$  on the surface is expressed by the following Boundary Integral equation (BIE),

$$u_i(\mathbf{x}_0) = -\frac{1}{4\pi\mu} \int_{S_B} [S_{ij}(\hat{\mathbf{x}})f_j(\mathbf{x}) - \mu T_{ijk}(\hat{\mathbf{x}})u_j(\mathbf{x})n_k(\mathbf{x})] dS \quad (2.3)$$

This equation relates the velocity  $\mathbf{u}$  at each point  $\mathbf{x}_0$  on the boundary  $S_B$  by the

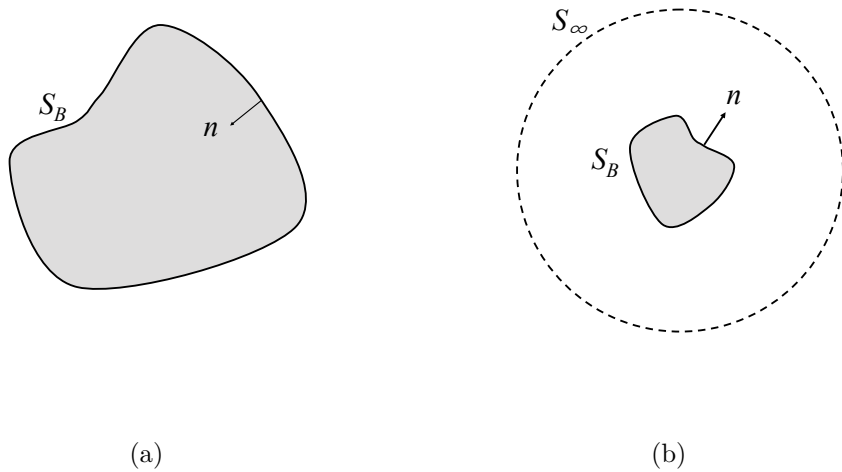


Figure 2.1: Illustrations for the geometry of the BIEs (2.3) and (2.15).

surface integral of the stress and velocity over all the points  $\mathbf{x}$  on the same boundary. The normal vector  $\mathbf{n}$  points into the domain surrounded by the boundary  $S_B$  while the force vector  $\mathbf{f}$  is defined by  $f_j(\mathbf{x}) = \sigma_{jk}(\mathbf{x})n_k(\mathbf{x})$ . The fundamental solution for the velocity  $S_{ij}$  and the corresponding stress  $T_{ijk}$  are given by

$$S_{ij} = \frac{\delta_{ij}}{r} + \frac{\hat{x}_i \hat{x}_j}{r^3} \quad (2.4)$$

$$T_{ijk} = -6 \frac{\hat{x}_i \hat{x}_j \hat{x}_k}{r^5} \quad (2.5)$$

where  $\hat{\mathbf{x}} = \mathbf{x} - \mathbf{x}_0$ . A detailed derivation may be found in Pozrikidis [33].

Equation (2.3) can be named as the “inner” equation because it solves for the fluid flow inside a specific boundary  $S_B$  shown in Figure 2.1(a). An “outer” equation can be derived to express the flow field outside a boundary  $S_B$  shown in Figure 2.1(b),

$$\mathbf{u}(\mathbf{x}_0) - 2\mathbf{u}^\infty(\mathbf{x}_0) = -\frac{1}{4\pi\mu} \int_{S_B} (\mathbf{S} \cdot \mathbf{f} - \mu \mathbf{T} \cdot \mathbf{u} \cdot \mathbf{n}) dS \quad (2.6)$$

where  $\mathbf{u}^\infty$  is the undisturbed fluid velocity and the normal vector  $\mathbf{n}$  points into the flow domain (i.e. out of the boundary  $S_B$ ).

## 2.2 BIE for a Droplet in a Channel

Boundary integral equation for the case of a droplet moving in a confined geometry (channel) can also be derived. As illustrated in Figure 2.2, the droplet fluid (fluid 1) has density  $\rho_1$  and viscosity  $\mu_1 = \lambda\mu$  and is confined in a channel. The outer fluid (fluid 2) has density  $\rho_2$  and viscosity  $\mu_2 = \mu$ . The flow velocity for fluid 1 and fluid 2 is denoted  $\mathbf{u}_1$  and  $\mathbf{u}_2$ , respectively. For the droplet interface  $S_d$ , the boundary conditions are

$$\mathbf{u} = \mathbf{u}_1 = \mathbf{u}_2 \quad (2.7)$$

$$\Delta \mathbf{f} \equiv \mathbf{f}_2 - \mathbf{f}_1 = \gamma(\nabla \cdot \mathbf{n})\mathbf{n} + (\rho_2 - \rho_1)(\mathbf{g} \cdot \mathbf{x})\mathbf{n} \quad (2.8)$$

where the subscripts “1” and “2” represent the internal and external flow, respectively. The interfacial tension  $\gamma$  is assumed to be constant and the magnitude of the gravity acceleration is  $g$ . For the boundary condition of the channel surface denoted  $S_2$ ,  $\mathbf{u}^\infty$  and stress  $\mathbf{f}^\infty$  are the undisturbed flow velocity and stress at the each end of the channel  $S_2^f$  which is assumed far enough from the droplet interface.  $S_2^w$  is the solid boundary (i.e. the channel and the constriction). Then the boundary conditions are

$$\mathbf{u}_2 = 0 \quad \text{on boundary } S_2^w \quad (2.9)$$

$$\mathbf{u}_2 = \mathbf{u}^\infty \quad \text{or} \quad \mathbf{f}_2 = \mathbf{f}^\infty \quad \text{on boundary } S_2^f \quad (2.10)$$

The normal vector  $\mathbf{n}$  at the interface  $S_d$  and the surface  $S_2$  points into fluid 2. The

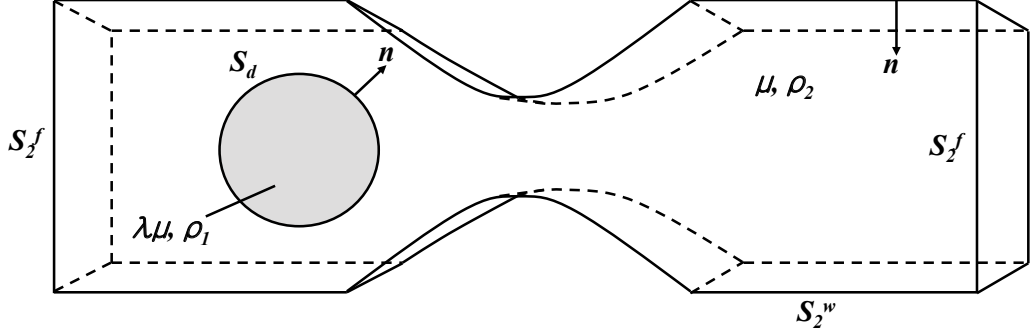


Figure 2.2: Illustration of a droplet in the fluid inside a channel with constriction.

droplet interior fluid is driven to flow by the exterior flow. Thus by applying the governing equation (2.3) on the fluid flow both inside and outside the drop, and then subtracting between the two equations, a general Boundary Integral equation for both flow regions can be derived as

$$\begin{aligned} \Omega \mathbf{u}(\mathbf{x}_0) &= - \int_{S_2} [\mathbf{S} \cdot \mathbf{f}_2 - \mu \mathbf{T} \cdot \mathbf{u}_2 \cdot \mathbf{n}] dS \\ &\quad - \int_{S_d} [\mathbf{S} \cdot \Delta \mathbf{f} - (1 - \lambda) \mu \mathbf{T} \cdot \mathbf{u} \cdot \mathbf{n}] dS \end{aligned} \quad (2.11)$$

For points on  $S_d$ ,  $\Omega = 4\pi(1 + \lambda)\mu$ ; for points on  $S_2$ ,  $\Omega = 4\pi\mu$ .

### 2.3 Dimensionless Parameters of the Current Problem

If the shear rate of the flow is below a certain critical value, the surface tension force and the external viscous force on the drop interface can balance each other, and a steady state can be reached. Otherwise the drop bursts and produces two or

more daughter droplets. The evolution of the droplet shape and the steady-state deformation are among the principal goals of both experimental and theoretical studies in this area.

The lengths are non-dimensionalized with the half length  $R$  of the side of the square channel, velocity with the average bulk velocity  $U$ , and time with  $R/U$ . The problem of interfacial dynamics in Stokes flow is governed by the viscosity ratio  $\lambda$ , the capillary number  $Ca$  and the droplet size  $a$  given by

$$\lambda = \frac{\mu_1}{\mu} \quad (2.12)$$

$$Ca = \frac{\mu U}{\gamma} \quad (2.13)$$

$$a = \tilde{a}/R \quad (2.14)$$

where  $\tilde{a}$  is the radius of a sphere with the same volume as the droplet. The capillary number  $Ca$  measures two competing forces: the viscous forces and the surface tension forces. The viscous stress imposed on the interface by the exterior flow induces the flow inside the drop and causes the interfacial deformation, while the surface tension forces resist the deformation. When steady state is reached, the surface tension forces balance the viscous forces and the droplet deformation ceases.

The steady unidirectional flow in the square channel far from the droplet is given as [52]

$$\frac{u_x^\infty}{C} = (1 - z^2) + \sum_{n=1}^{\infty} B_n \cosh(\alpha_n y) \cos(\alpha_n z) \quad (2.15)$$

where

$$C = \frac{-(\Delta p/\Delta x)}{2\mu} \quad (2.16)$$

$$B_n \cosh(\alpha_n) = (-1)^n \frac{4}{\alpha_n^3} \quad (2.17)$$

$$\alpha_n = \frac{(2n-1)\pi}{2} \quad (2.18)$$

The variables  $y$  and  $z$  are non-dimensionalized with the channel size  $R$ . The flow rate  $Q$  and the average velocity  $U$  in the channel are given by

$$\frac{Q}{C} = \frac{8}{3} + \sum_{n=1}^{\infty} (-1)^n \frac{16}{\alpha_n^5} \sin(\alpha_n) \tanh(\alpha_n) \quad (2.19)$$

$$\frac{U}{C} = \frac{Q}{AC} = \frac{2}{3} + \sum_{n=1}^{\infty} (-1)^n \frac{4}{\alpha_n^5} \sin(\alpha_n) \tanh(\alpha_n) \quad (2.20)$$

where  $A$  denotes the non-dimensionalized cross-sectional area of the square channel. In our computations, the infinite series in equation (2.15) is cut off after  $n=40$  with a truncation error of  $O(10^{-5})$ .

## 2.4 Rest Physical Variables of Interest

For our results, we obtain five main quantities; droplet velocity, the deformation of the droplet in  $x, y, z$  directions, the surface area of the droplet and the minimum distance between the droplet and the solid surfaces.

We calculate the length  $L_x$ , the width  $L_y$  and the height  $L_z$  of the droplet as the maximum distance in the  $x, y, z$  coordinates of the droplet surface as illustrated in Fig(b). We employ a Newton's method for the optimization.

The minimum distance between the droplet surface and the solid surface  $h_{min}$  is calculated using a Newton's method for the optimization.

# Chapter 3

## Numerical Method for Interfacial Dynamics

### 3.1 Spectral Element Formulation

In this thesis, we utilize the fully-implicit three-dimensional Spectral Boundary Element method developed by Dimitrakopoulos [11]. According to this method, the problem boundary is divided into a moderate number  $N_E$  of surface elements, each of which is mapped onto a two-dimensional domain in terms of the parametric variables  $\xi$  and  $\eta$ . The variables are zeros of orthogonal polynomials, such as Legendre, Chebyshev or Jacobi polynomials, on  $[-1, 1]$ . If  $N_B$  basis points are used, then the geometry  $\mathbf{x}$  can be represented by

$$\mathbf{x}(\xi, \eta) = \sum_{i=1}^{N_B} \sum_{j=1}^{N_B} \mathbf{x}(\xi_i, \eta_j) h_j(\eta) h_i(\xi) \quad (3.1)$$

where  $h_i(\xi)$  and  $h_j(\eta)$  are the  $(N_B - 1)$ -order Lagrangian interpolant polynomial. The physical variables  $\mathbf{u}$  and  $\mathbf{f}$  are represented similarly.

The discretized expressions for the geometry and the physical variables are substituted into the boundary integral equations which it is required that the integral equations be satisfied at the discrete set of basis points  $\mathbf{x}_0(\xi_i, \eta_j)$ , where  $i, j =$

$1, 2, \dots, N_B$ . This yields a linear system of  $3N_EN_B^2$  algebraic equations

$$\mathbf{u} = \mathbf{A}\mathbf{f} + \mathbf{B}\mathbf{u} \quad (3.2)$$

The system matrices  $\mathbf{A}$  and  $\mathbf{B}$  are defined as integrals of the kernels  $\mathbf{S}$  and  $\mathbf{T}$  (equations 2.4, 2.5) and the basis functions over the set of the surface elements. The numerical integration is performed by Gauss-Legendre quadrature with the aid of variable transformations. Owing to the singularity in the kernels, special care must be taken to ensure the accurate numerical evaluation of these integrations [6, 11].

The BIEs, combined with the boundary data at the  $N_EN_B^2$  basis points, yield, for a known interface, a consistent set of  $3N_EN_B^2$  equations in  $3N_EN_B^2$  unknowns which is solved using Gaussian elimination.

### 3.2 Explicit Time-integration Algorithm

We consider a three-dimensional droplet suspended in an infinite fluid undergoing a low-Reynolds-number flow. The governing equations are the Stokes equations along with the continuity equation. The corresponding Boundary Integral equation (2.11) and the boundary conditions (2.7) - (2.8) described in Section 2.2. The drop interface is discretized into  $N_E$  elements with  $N_B \times N_B$  spectral basis points on each element. These points are of Lobatto type, i.e. end points along with interior points. For a given droplet geometry, the velocity on the droplet interface is obtained by the Spectral Boundary Element method described in Section 3.1.

In order to determine the shape  $\mathbf{x}(t)$  of the drop as a function of time, a time-

integration algorithm is employed to solve the kinematic condition at the interface, which has the general form

$$\frac{d\mathbf{x}}{dt} = (\mathbf{u} \cdot \mathbf{n})\mathbf{n} + U_t \mathbf{t} \quad (3.3)$$

The first term on the right hand side is the contribution of the normal interfacial velocity which determines the interfacial shape of the droplet. The second term denoting the contribution of a velocity tangential to the interface, only affects the distribution of the spectral points along the interface.

Thus, we determine the interfacial velocity  $\mathbf{u}$  of the known shape  $\mathbf{x}(t)$  from BIE (2.11), and then the discretized points of the droplet interface are advanced by a time interval  $\Delta t$  to obtain the shape  $\mathbf{x}(t + \Delta t)$ . An explicit high-order Runge-Kutta method is employed for the time-integration. We note that explicit time-integration schemes have commonly been employed with various discretization methods, e.g. Leyrat-Maurin, and Barthes-Biesel [26], Griggs, Zinchenko and Davis [18], Janssen and Anderson [23] and Jensen, Stone and Henrik Bruus [24].

However, for any explicit scheme, the employed time step  $\Delta t$  needs to satisfy the Courant condition to have numerical stability. The dimensionless form of the Courant condition may be written as

$$\Delta t < 0(Ca\Delta x_{min}) \quad (3.4)$$

where  $\Delta x_{min}$  represents the minimum length scale (e.g. grid size). For the problem of a droplet squeezing through a constriction, the thin film between the droplet and the solid limits the time step to be very small.

### 3.3 Implicit Time-integration Algorithm

In order to avoid the penalty of small time steps required by the Courant condition, we employ an efficient fully-implicit spectral boundary element algorithm for interfacial dynamics in Stokes flow developed by Dimitrakopoulos[11]. The method is based on a mathematically rigorous combination of implicit schemes with a Jacobian-free three-dimensional Newton method. Thus the algorithm has the essential stability property of the implicit formula and allows very large time steps regardless of the grid density.

For the current problem, we utilized the third-order diagonally-implicit Runge-Kutta scheme to achieve sufficient accuracy shown in Table 3.1. The accuracy of our results has been verified by comparing different time steps ( $\Delta t = 0.01, 0.025$  and  $0.05$ ) and basis points  $N_B = 10, 12$ .

Table 3.1: Diagonally-implicit Runge-Kutta (DIRK) scheme of third order [11]

---

$$\begin{aligned}\mathbf{x}_{s1} &= \mathbf{x}_n + \Delta t b_0 \mathbf{a}(\mathbf{x}_{s1}) \\ \mathbf{x}_{s2} &= \mathbf{x}_n + \Delta t [0.5(1 - b_0) \mathbf{a}(\mathbf{x}_{s1}) + b_0 \mathbf{a}(\mathbf{x}_{s2})] \\ \mathbf{x}_{n+1} &= \mathbf{x}_n + \Delta t [b_1 \mathbf{a}(\mathbf{x}_{s1}) + b_2 \mathbf{a}(\mathbf{x}_{n+1})]\end{aligned}$$

---

### 3.4 Spectral Boundary Element Discretization of a Droplet in a Channel

A demonstration of the discretization of the channel geometry is shown in Figure 3.1. Note that 4 elements are defined for each row on the solid geometry while 2 rows of element are used for the constriction. The fluid boundary in the inlet and outlet of the channel is composed of one element on each side. In order to account for the undisturbed velocity at the end, the half-length of the channel is defined at least 9 times longer than the half-size of the channel's side  $R$ . Our convergence runs showed negligible error for this length.

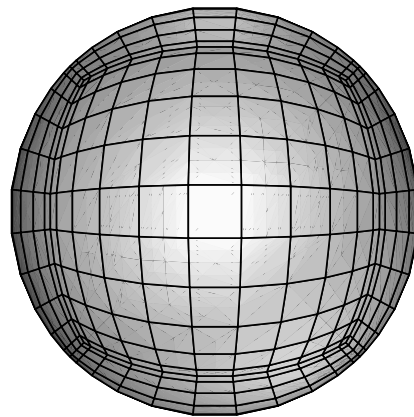
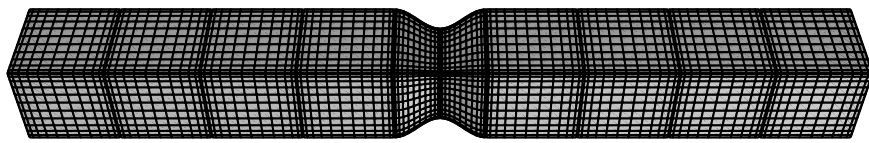


Figure 3.1: Spectral Boundary Element discretization of a channel and a droplet.

# Chapter 4

## Results and Discussion

In this chapter, we first validate our method by comparing our results with findings from previous studies. Then we examine the motion of a droplet squeezing through a rectangularly-constricted square channel from various aspects, starting with the comparison between the square and the rectangular constriction. Afterwards, we determine the effects of the capillary number, viscosity ratio, constriction length and constriction gap size on the droplet velocity, deformation, and droplet-solid minimum gap.

### 4.1 Validation

We validate our numerical algorithm for droplet dynamics in capillary tubes by comparing our data with those of previous studies. Figure 4.1 shows the comparison of our results for the droplet motion in a cylindrical tube with the previous studies of the same geometry and conditions. For capillary number  $Ca$  ranging from 0.075 to 0.15 and viscosity ratio  $\lambda$  from 0.001 to 10, our data (solid dots) are found to be in excellent agreement with previous results [45, 28].

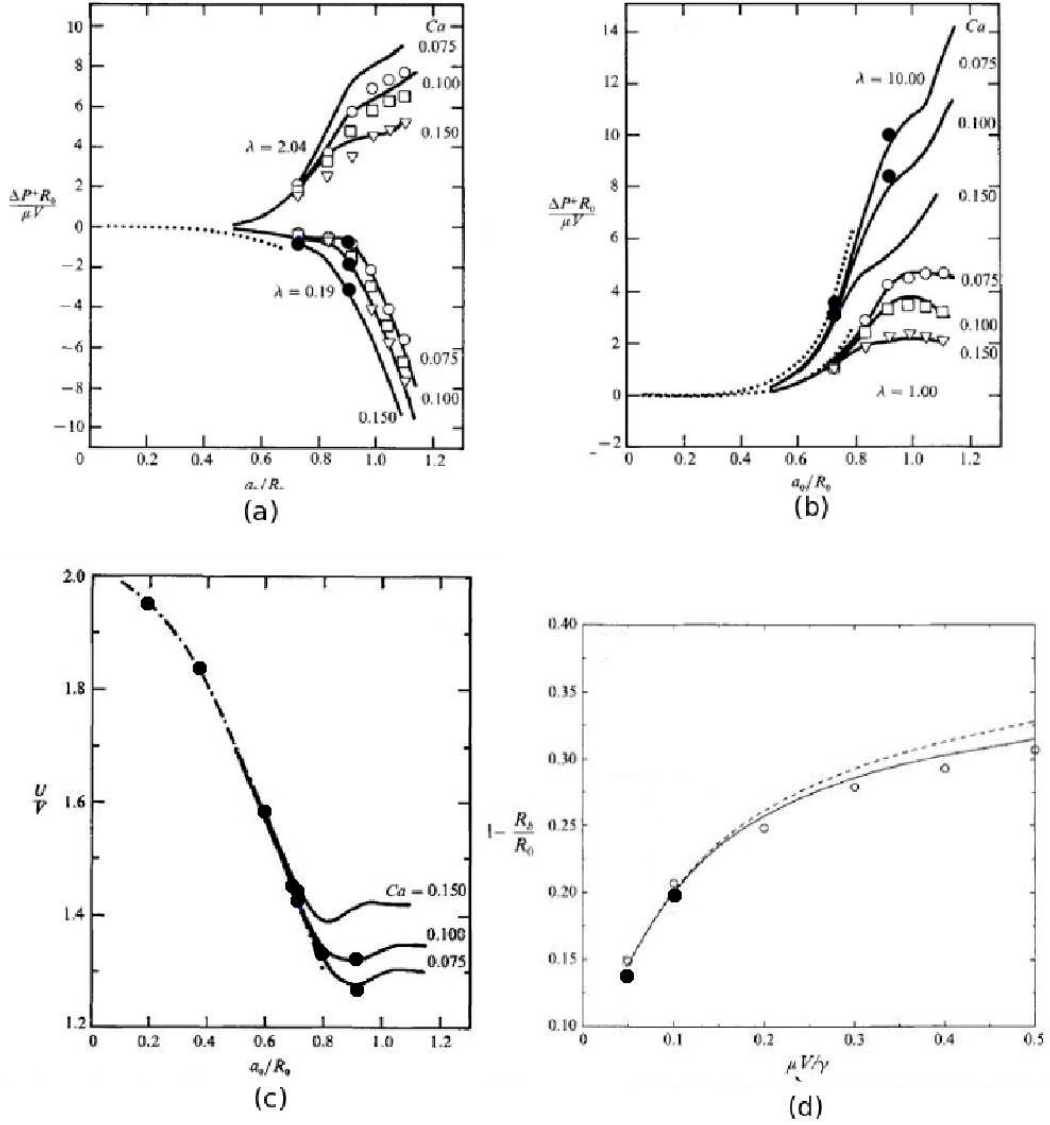


Figure 4.1: Validation of our algorithm by comparison with previous studies: (a),(b),(c) from Tsai and Miksis [45] and (d) from Martinez and Udell [28]. The solid dots represent our data.

## 4.2 Rectangular and Square Constriction

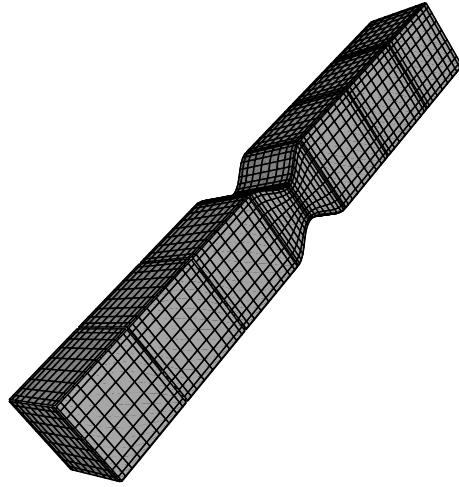
We first decide our standard case of a droplet squeezing through a rectangular constriction in a square channel. For our standard case, the cross-sectional dimension of the channel is defined as  $y \times z = 2 \times 2$  with the minimum gap of the full-cosine constriction equals to 1.0 and defined only on  $z$ -axis. Thus the cross-sectional dimension of the rectangular constriction is  $y \times z = 2 \times 1$  at its minimum. The length of the constriction is 1.0 and the constriction is located at the center of the channel  $x = 0$ . A droplet of radius  $a = 0.6$  is initially placed at  $X_c = -3.0$  where  $X_c$  is the droplet's center of mass. The rest problem parameters are: capillary number  $Ca = 0.1$  and viscosity ratio  $\lambda = 5$ . A three-dimensional shape of the geometry is shown in Figure 4.2(a).

The comparing case of a droplet squeezing through a square constriction has the same parameters as the rectangular constriction but now the cross-sectional dimension of the constriction is  $y \times z = 1 \times 1$ . Thus it has symmetry on  $y, z$  and  $yz$ -axis throughout the computation. A three-dimensional shape of this geometries is shown in Figure 4.2(b).

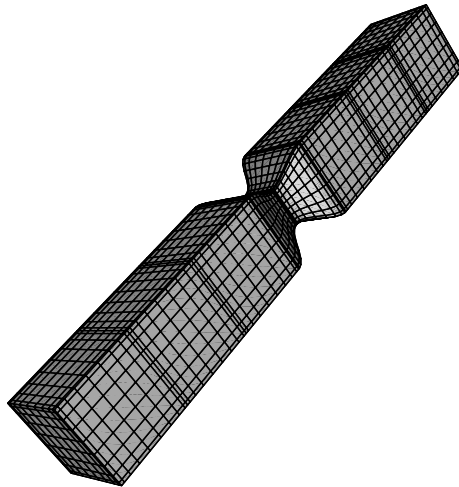
In Figure 4.3 we plot the droplet velocity in the flow direction  $U_x$  versus the its center of mass  $X_c$  and  $X_c$  versus time  $t$ . We can see that the droplet travels faster in the square constriction with its maximum velocity reaching more than twice the velocity of the droplet in the rectangular constriction. Note that the flow rate of the outer fluid in the middle of the square constriction is exactly twice the flow rate of in the middle of the rectangular constriction. The higher increase of the droplet

velocity is induced by the deformation of its shape.

The evolution of the droplet shapes in the rectangular and the square constrictions are shown in Figure 4.4 and Figure 4.5. In Figure 4.4 where the two-dimensional droplet shapes in  $y$ -axis view are drawn at time  $t = 0, 1, 1.25, 1.5, 1.75, 2, 3$ , we see that the droplet velocity in the square constriction increases earlier and higher by the larger deformation of the droplet, starting at the nose of the droplet followed by the rear. In Figure 4.5, we can see the evolution of the three-dimensional droplet shapes in  $y$  and  $z$ -axis view. The droplet at its centroid positions  $X_c = -0.5, 0, 0.5$  are drawn to see the major differences of the deformation. Clearly the  $x$ -length of the droplet in the square constriction increases much longer while the droplet in rectangular constriction is able to extend in  $y$ -direction. However the magnitude of extension in the  $y$ -direction is minor.



(a) Rectangular constriction



(b) Square constriction

Figure 4.2: Perspective of square channels with (a) a rectangular and (b) a square full-cosine constriction of 1.0 length and 1.0 minimum gap.

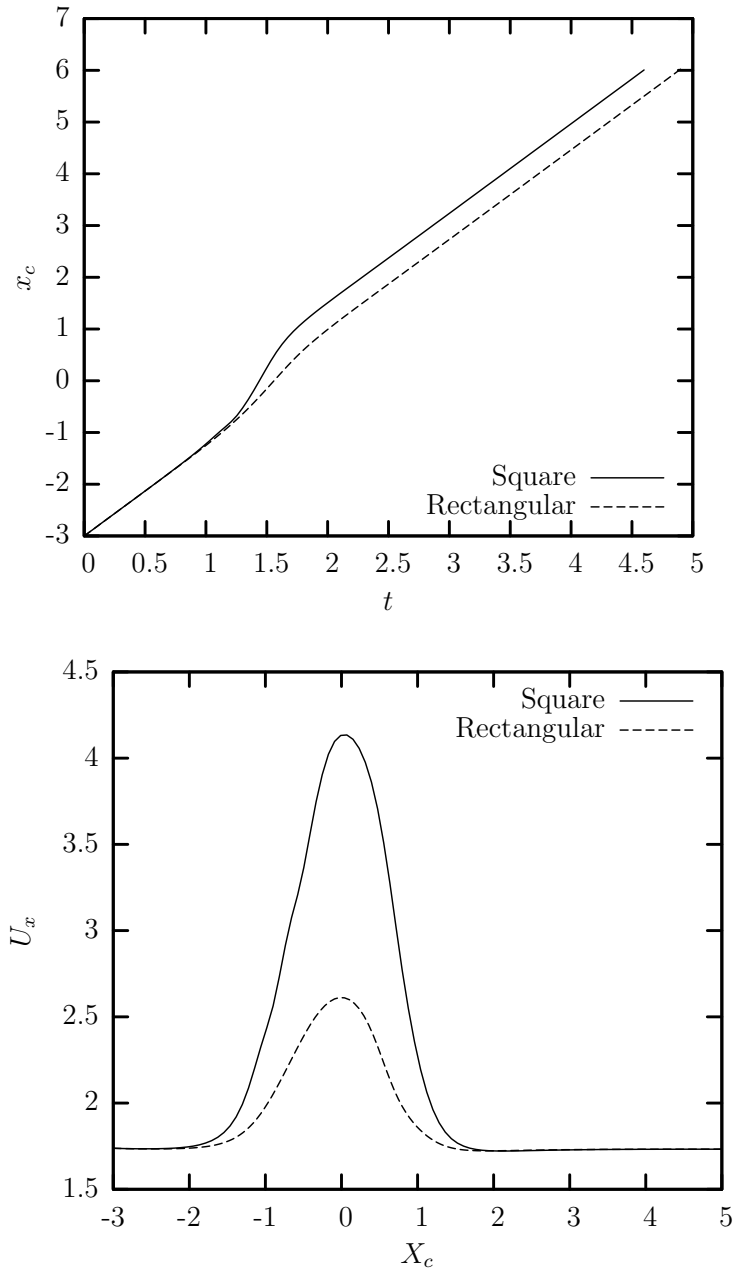


Figure 4.3: (a) Droplet centroid  $X_c$  versus time  $t$  and (b) droplet velocity  $U_x$  versus its centroid  $X_c$  for a droplet with  $a = 0.6$ ,  $Ca = 0.1$  and  $\lambda = 5$  squeezing through a rectangular and a square full-cosine constriction with 1.0 length and 1.0 minimum gap.

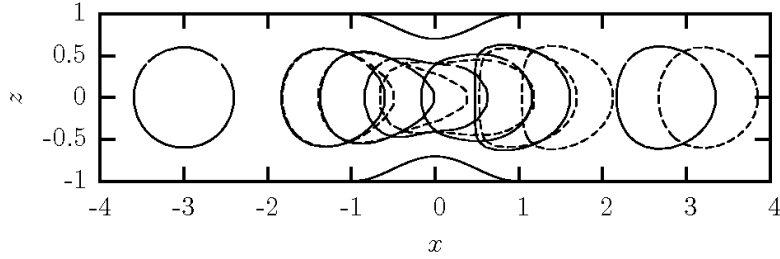


Figure 4.4: Evolution of the droplet profile with  $Ca = 0.1$ ,  $\lambda = 5$ ,  $a = 0.6$ , at  $t = 0, 1, 1.25, 1.5, 1.75, 2.0, 3$  squeezing through a rectangular and a square full-cosine constriction with 1.0 length and 1.0 minimum gap ( $y$ -axis view).

It is more feasible to study the deformation by looking at Figure 4.6 and Figure 4.7 where the droplet's length in the  $x$ ,  $y$ ,  $z$  coordinates are plotted. Unlike the square constriction, the asymmetric rectangular constriction geometry enables the droplet to stay extended in  $y$ -axis as shown in Figure 4.6(b). Thus when the droplet is entering and passing through the constriction it doesn't have to deform as much in  $x$ -direction. At the exit of the constriction the droplet experiences compression in the flow direction and expansion in the  $z$ -direction. When the droplet is escaping the constriction, the velocity of the droplet's nose decreases rapidly while the rear part of the droplet is still inside the constriction and moving fast. The velocity difference in the flow direction causes the droplet to expand in  $z$ -axis in order to maintain the incompressible fluid condition. However the droplet doesn't expand in  $y$ -axis but rather is compressed. This is because the expansion in  $z$ -axis is more significant due to the outer fluid flow direction. The outer fluid profile

near the constriction wall points along the shape of the constriction. In  $z$ -direction, the droplet surface near the solid surface experiences shear force parallel to the constriction wall thus the droplet prefers to expand in  $z$ -axis much more. After droplet has completely passed the constriction, the droplet deforms towards its steady-state shape.

Figure 4.8(a) shows the surface area  $S_d$  of the droplet versus its centroid  $X_c$ . In current study, the droplet's surface area  $S_d$  is used as to measure the overall magnitude of deformation. The droplet squeezing through the rectangular constriction shows smaller overall deformation owing to the wider constriction gap and slower droplet velocity.

Figure 4.8(b) shows the minimum drop-solid distance  $h_{min}$  versus  $X_c$ . Surprisingly, the minimum gap is smaller for the rectangular constriction. Owing to the slower droplet velocity and its smaller deformation, the droplet squeezing through rectangular constriction shows thinner film between the droplet and the bump. The discontinuities before and after the droplet-solid minimum gap indicate that the minimum gap position changed from the straight channel to constriction, or vice versa.

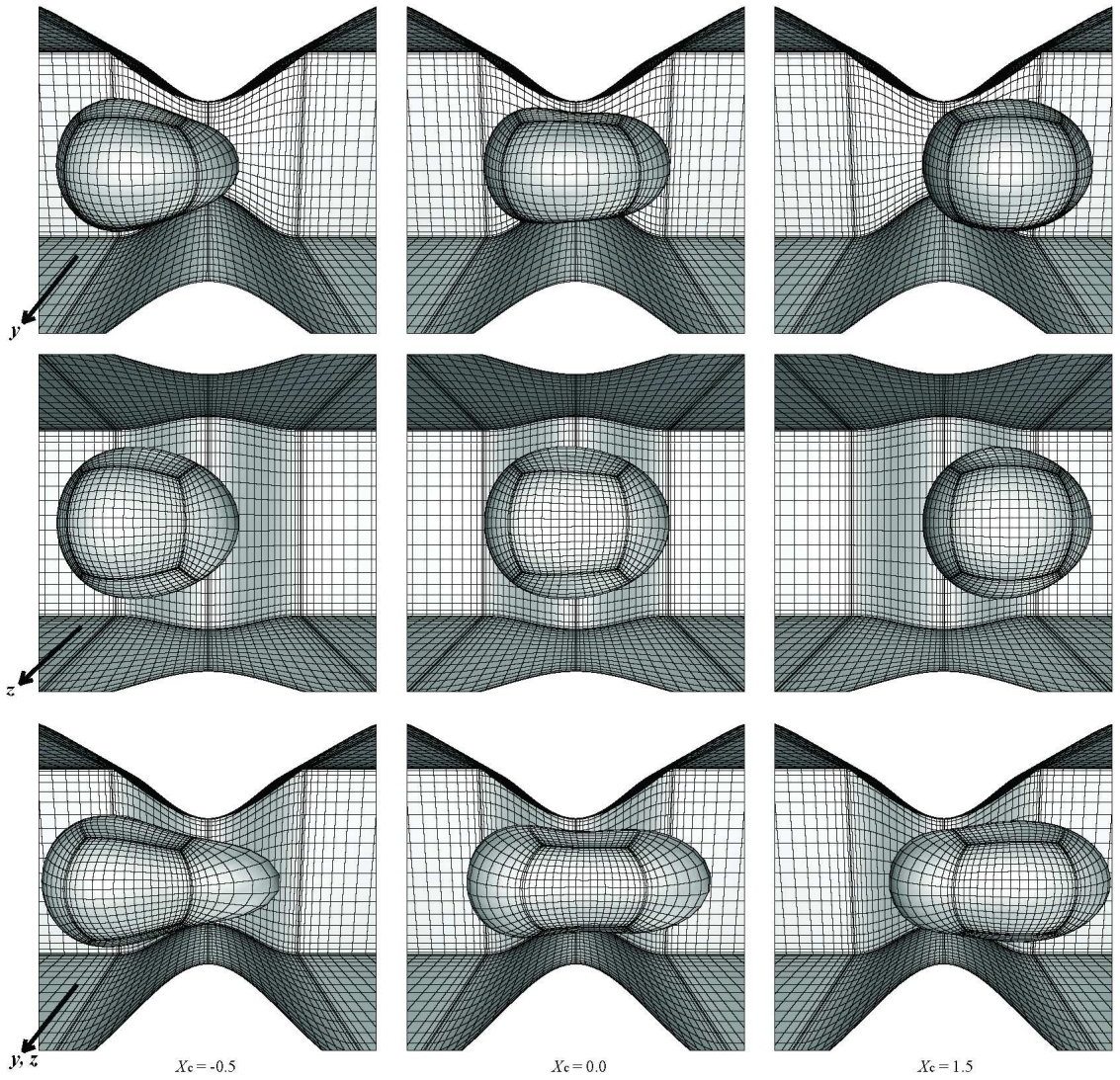


Figure 4.5: Three-dimensional  $y$  and  $z$ -axis shapes of the droplets with  $a = 0.6$ ,  $Ca = 0.1$ ,  $\lambda = 5$ , at  $X_c = -0.5, 0, 0.5$ , squeezing through a rectangular and a square full-cosine constriction with 1.0 length and 1.0 minimum gap.

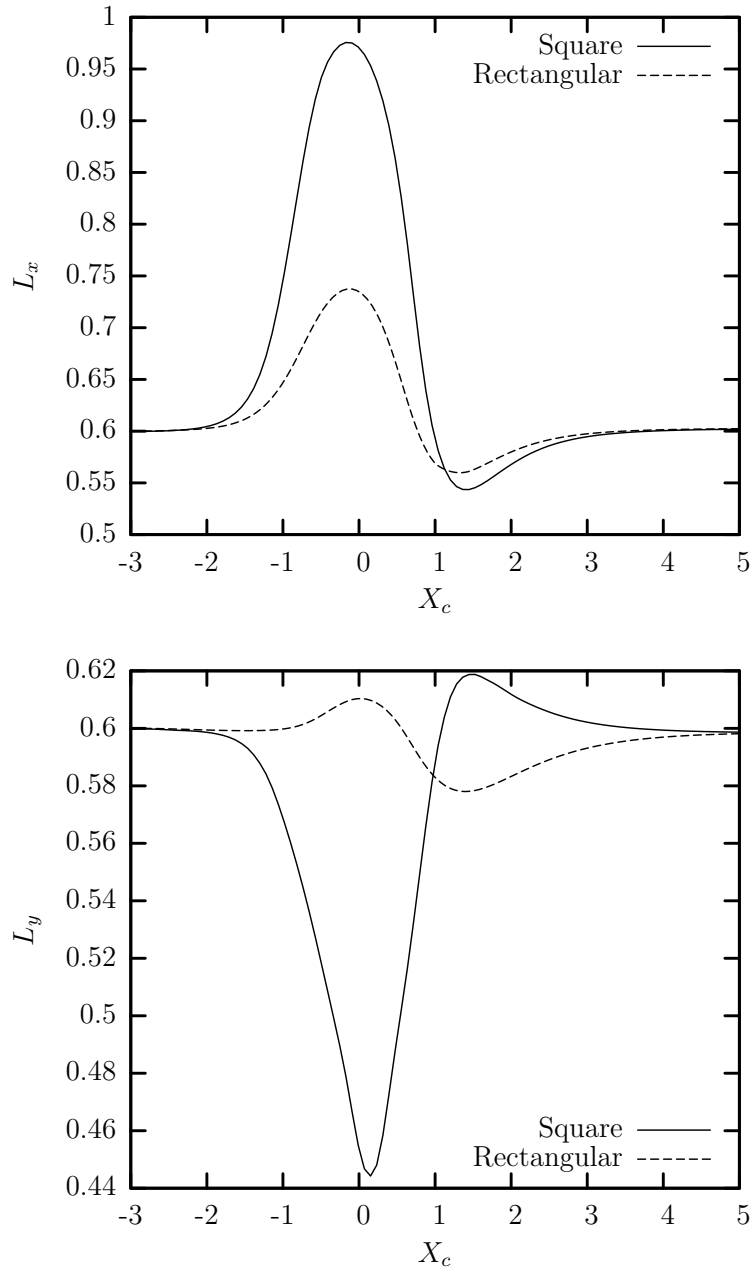


Figure 4.6: (a) Droplet  $x$ -length  $L_x$  and (b)  $y$ -length  $L_y$  versus its centroid  $X_c$  for a droplet with  $a = 0.6$ ,  $Ca = 0.1$  and  $\lambda = 5$  squeezing through a rectangular and a square full-cosine constriction with 1.0 length and 1.0 minimum gap.

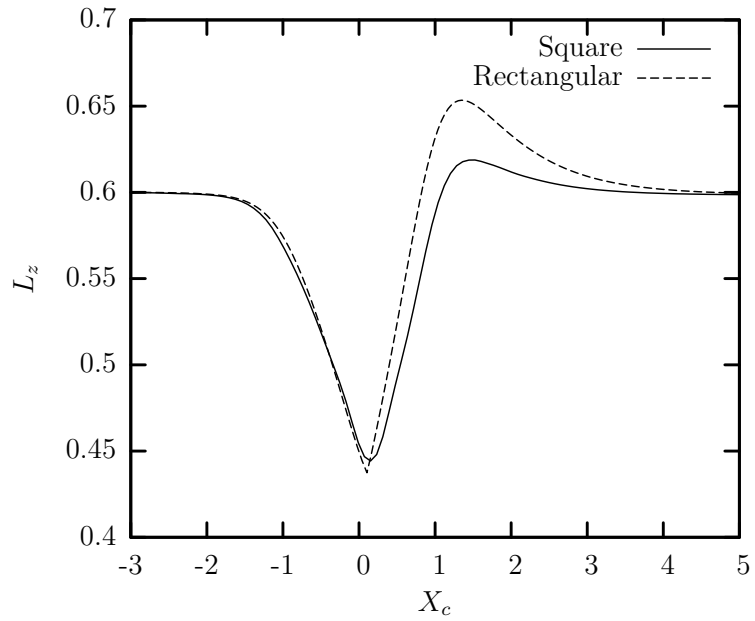


Figure 4.7: Droplet  $z$ -length  $L_z$  versus its centroid  $X_c$  for a droplet with  $a = 0.6$ ,  $Ca = 0.1$  and  $\lambda = 5$  squeezing through a rectangular and a square full-cosine constriction with 1.0 length and 1.0 minimum gap.

### 4.3 Rectangular Constriction

In this section, we consider the effects of several parameters on a droplet squeezing through a rectangular constriction in a square channel. The parameters include the capillary number  $Ca$ , the viscosity ratio  $\lambda$ , the constriction length and the constriction gap size. Again the effects of each parameters are investigated using the shapes of the droplet and the plots of droplet's centroid  $X_c$ , droplet's velocity in the flow direction  $U_x$ , droplet's surface area  $S_d$  and minimum gap between the droplet and the solid  $h_{min}$ .

#### 4.3.1 Effects of Capillary Number

Now we vary the capillary number while keeping all other parameters fixed. The three capillary numbers we investigated are  $Ca = 0.05, 0.1, 0.2$ . Previous studies have reported that large capillary number droplets in a straight tube do not have steady state solution. A droplet of  $a = 0.9$  showed jetting behavior at  $Ca = 1.0$  [45] and for  $a = 0.726$ , at  $Ca = 0.75$  [28]. Thus we stay away from these values to eliminate other effects. The viscosity ratio is fixed at  $\lambda = 5$ , the droplet size at  $a = 0.6$ , the constriction length at 1.0 and the minimum gap is 1.0.

As shown in Figure 4.10, the velocity increases as the capillary number is increased but the effect is not significant in the current range of the capillary number. Due to the droplet surface closer to the solid wall, lower capillary number droplets has more drag force causing the droplet to be slower. On the other hand, the smaller gap also indicates the outer fluid will have higher velocity. Nevertheless the velocity

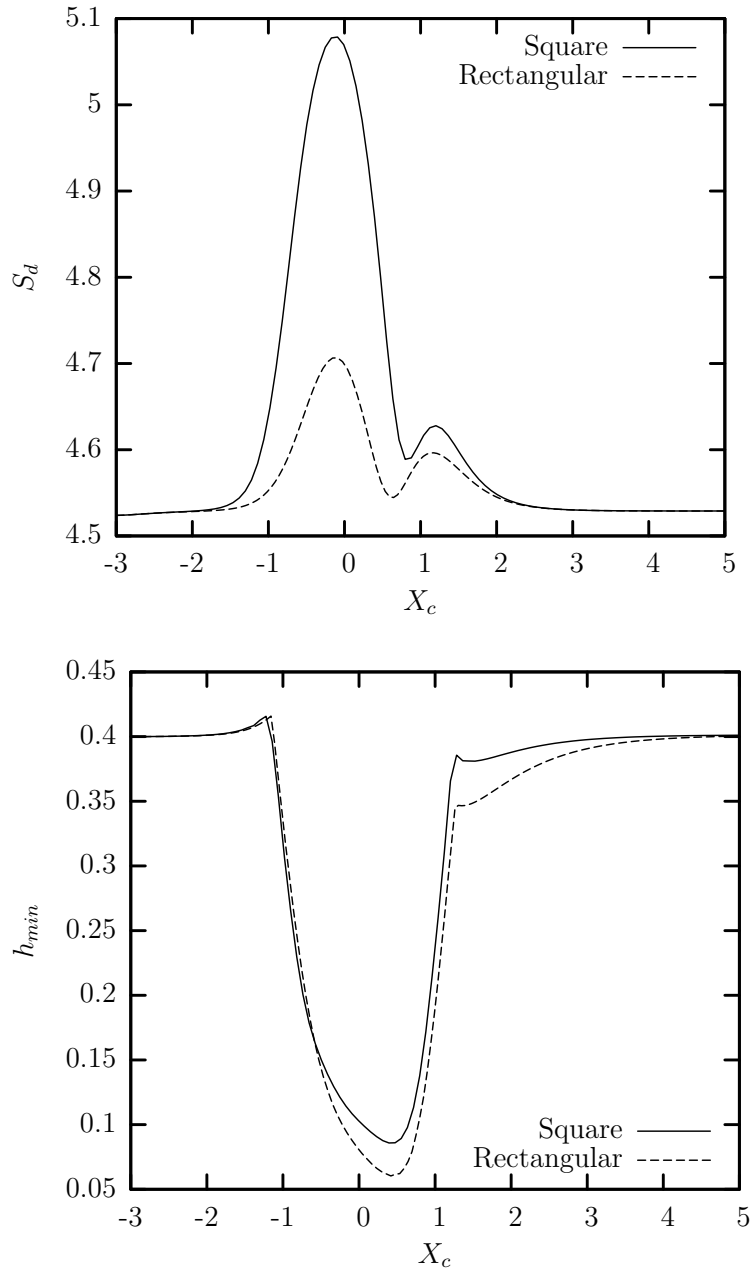


Figure 4.8: (a) Droplet surface area  $S_d$  and (b) droplet-solid minimum distance  $h_{min}$  versus its centroid  $X_c$  for a droplet with  $a = 0.6$ ,  $Ca = 0.1$  and  $\lambda = 5$  squeezing through a rectangular and a square full-cosine constriction with 1.0 length and 1.0 minimum gap.

decrease due to drag force exerts stronger influence as shown in the figure.

Figure 4.11 and Figure 4.12(a) show the projection lengths of the droplet in  $x, y, z$ -coordinates. At the upstream of the constriction, the droplet's  $x$ -length  $L_x$  increases as the capillary number is increased while its  $z$ -length  $L_z$  decreases. The lower capillary number droplets having higher surface tension, require more energy to deform from its spherical shape and thus deform less. This can be readily seen in Figure 4.13(a) where the droplet with the lowest capillary number has the minimum surface area.

At the downstream of the constriction, the lower capillary number droplets experience compression on  $x, y$ -axes and the expansion on  $z$ -axis with the same reason as described above. In Figure 4.13(a), the second maximum of the droplet's surface area is smaller for the lower capillary number droplets showing that the dominant factor is the surface tension. Also the droplets existing the constriction show different rates of deformation. The lower capillary number droplets deform more quickly.

We observed a dimple at the rear of the droplet, namely a "heart-shape" of the droplet at the downstream of the constriction for capillary number 0.1 and 0.2. Figure 4.15 shows the three-dimensional shape of the droplet at the droplet's centroid  $X_c = 1.3$ .

In Figure 4.13(b), we plot the minimum distance between the droplet and the solid. We can see as the capillary number decreases, the gap between the two surfaces becomes very thin down to  $h_{min} = 0.031$  which is less than 6% of its spherical radius. We again emphasize that the computation of a close surface to

surface interaction is numerically difficult to solve. In Figure 4.14, we can see that the size of the droplet-solid minimum distance is close to the grid sizes of the geometries. We also notice the minimum gap is obtained when the droplet's centroid is slightly down the downstream of the constriction at  $X_c = 0.47$ .

Figure 4.9 shows the three-dimensional shapes of the droplets of  $Ca = 0.05, 0.1, 0.2$  at  $X_c = 0$  view in  $y$  and  $z$ -axes.

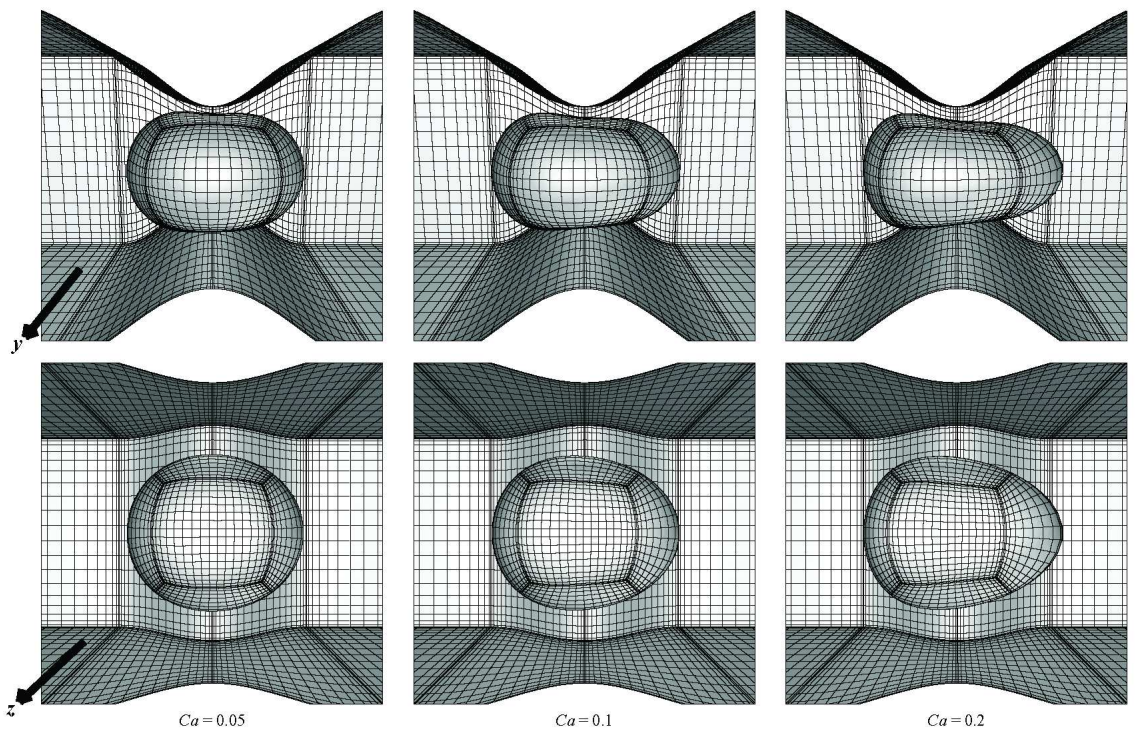


Figure 4.9: Three-dimensional  $y$  and  $z$ -axis shapes of the droplets with  $a = 0.6$ ,  $Ca = 0.05, 0.1, 0.2$ ,  $\lambda = 5$ , at  $X_c = 0$ , squeezing through a rectangular full-cosine constriction with 1.0 length and 1.0 minimum gap.

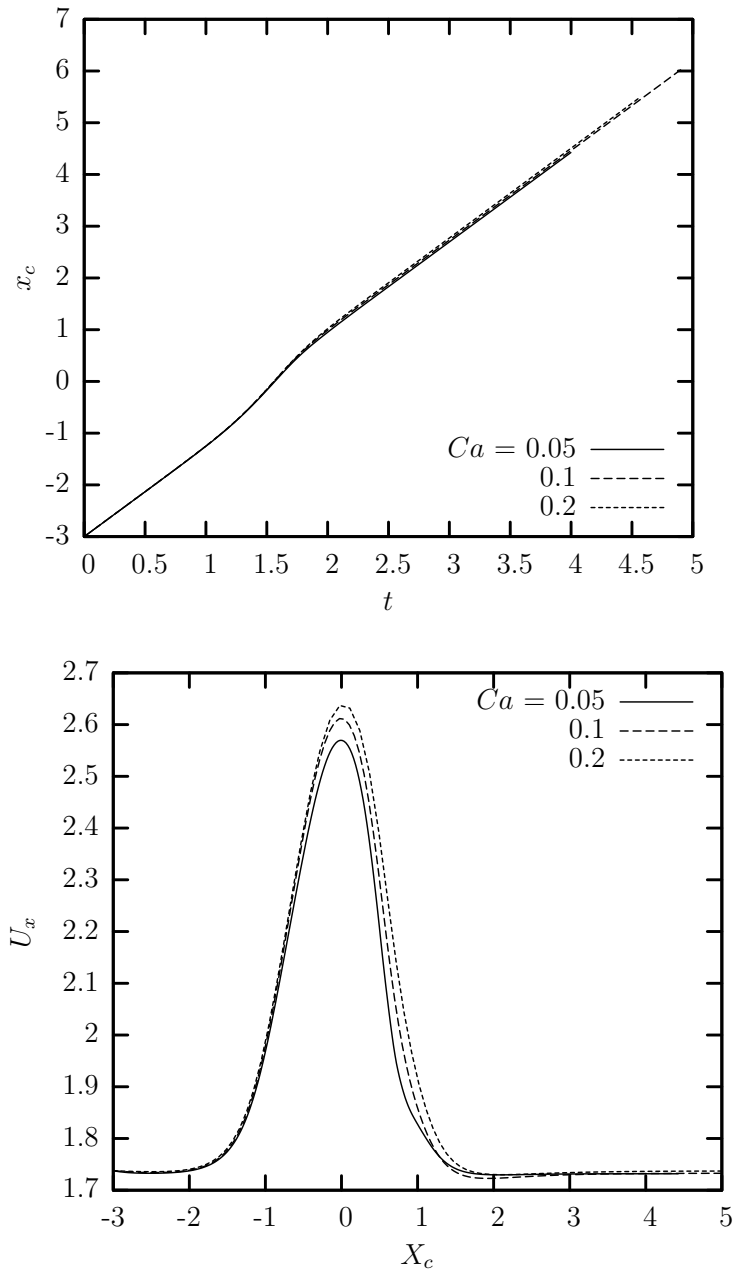


Figure 4.10: (a) Droplet centroid  $X_c$  versus time  $t$  and (b) droplet velocity  $U_x$  versus its centroid  $X_c$  for a droplet with  $a = 0.6$ ,  $Ca = 0.05, 0.1$  and  $0.2$  and  $\lambda = 5$  squeezing through a rectangular full-cosine constriction with  $1.0$  length and  $1.0$  minimum gap.

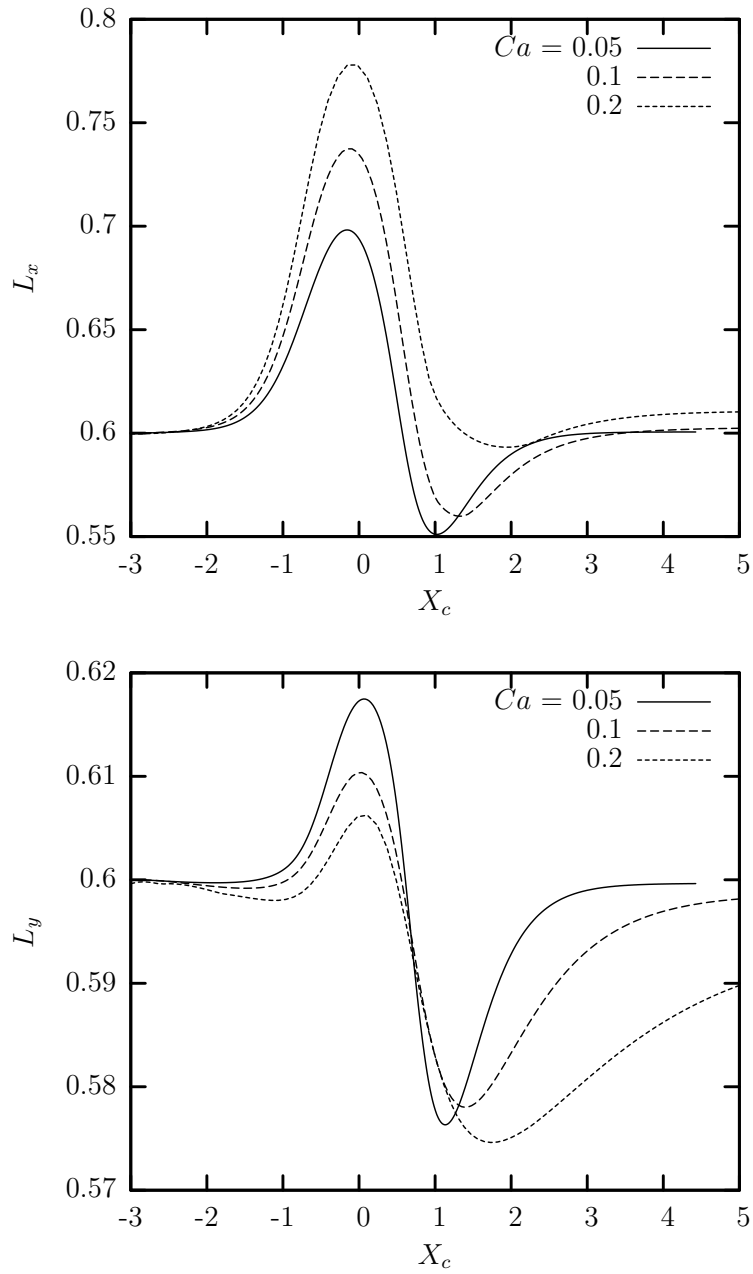


Figure 4.11: (a) Droplet  $x$ -length  $L_x$  and (b)  $y$ -length  $L_y$  versus its centroid  $X_c$  for a droplet with  $a = 0.6$ ,  $Ca = 0.05, 0.1$  and  $0.2$  and  $\lambda = 5$  squeezing through a rectangular full-cosine constriction with  $1.0$  length and  $1.0$  minimum gap.

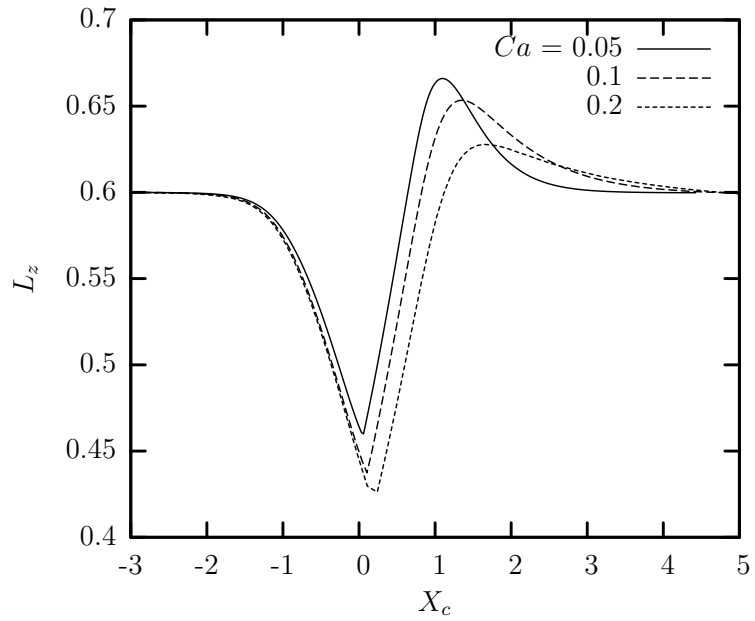


Figure 4.12: Droplet  $z$ -length  $L_z$  versus its centroid  $X_c$  for a droplet with  $a = 0.6$ ,  $Ca = 0.05, 0.1$  and  $0.2$  and  $\lambda = 5$  squeezing through a rectangular full-cosine constriction with  $1.0$  length and  $1.0$  minimum gap.

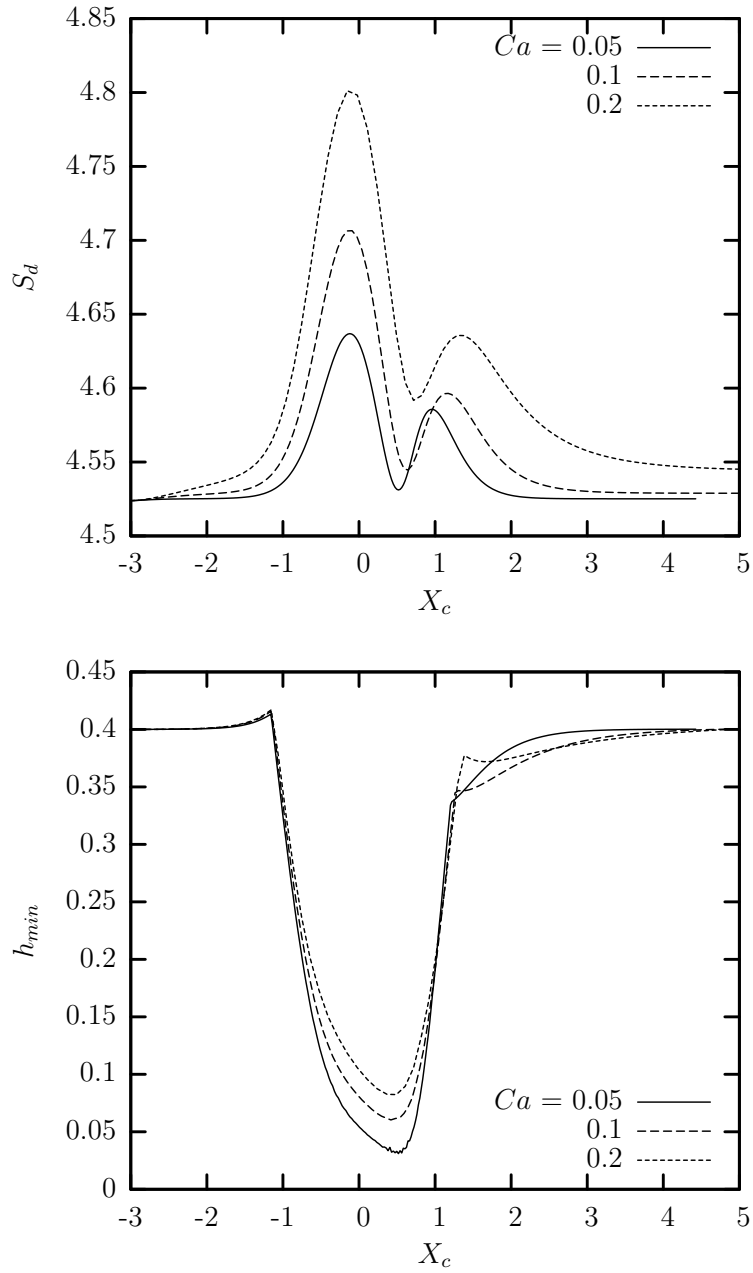


Figure 4.13: (a) Droplet surface area  $S_d$  and (b) droplet-solid minimum distance  $h_{min}$  versus its centroid  $X_c$  for a droplet with  $a = 0.6$ ,  $Ca = 0.05, 0.1$  and  $0.2$  and  $\lambda = 5$  squeezing through a rectangular full-cosine constriction with  $1.0$  length and  $1.0$  minimum gap.

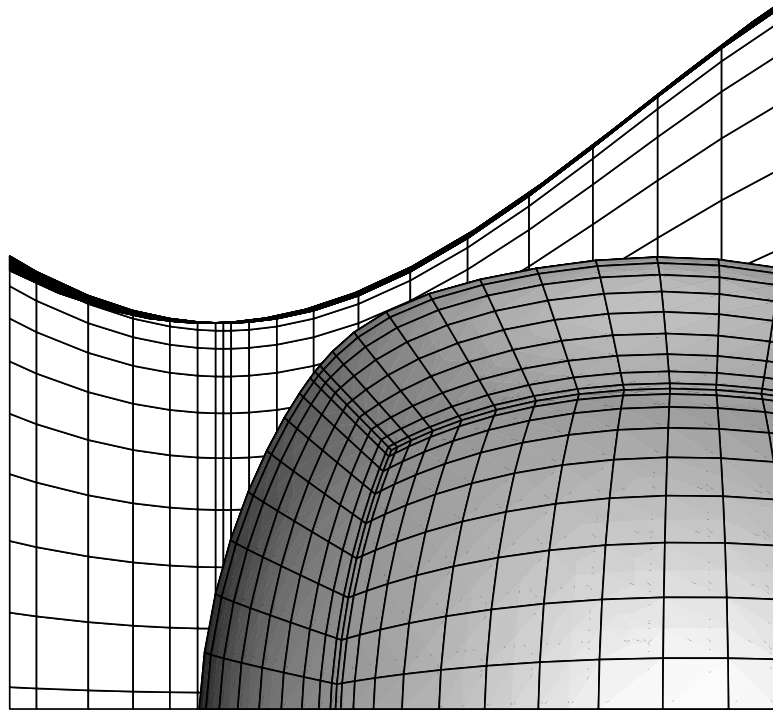


Figure 4.14: Minimum distance between the droplet and the solid  $h_{min} = 0.031$  at  $X_c = 0.47$  for a droplet with  $a = 0.6$ ,  $Ca = 0.05$  and  $\lambda = 5$  squeezing through a rectangular full-cosine constriction with 1.0 length and 1.0 minimum gap.

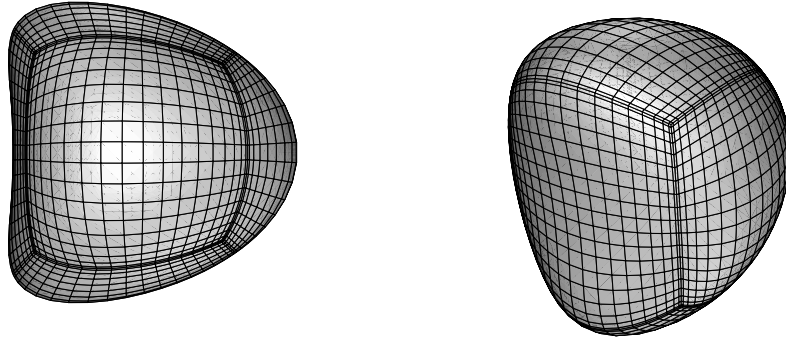


Figure 4.15: Three-dimensional shape of a droplet with  $a = 0.6$ ,  $Ca = 0.2$ ,  $\lambda = 5$  forming a dimple at the rear-part of the droplet at its centroid  $X_c = 1.3$  (heart-shape).

### 4.3.2 Effects of Viscosity Ratio

Now we compare the effects of viscosity ratios on the droplet squeezing through the rectangular constriction in a square channel. We use five viscosity ratios  $\lambda = 0, 0.1, 1, 5$  and  $10$  with fixed capillary number  $Ca = 0.1$ , minimum gap constriction of  $1.0$  and droplet size  $a = 0.6$ . Most of the graphs, we plotted three viscosity ratios ( $\lambda = 0, 1, 10$ ) for visuality although the discussion is made for all five values.

On Figure 4.17, we plot the velocity of the droplet  $U_x$  respect to the position of the droplet  $X_c$  and the position of the droplet centroid  $X_c$  versus time  $t$ . Higher viscosity ratio droplet starts with lower velocity and moves slower through the constriction. Due to higher hydrodynamic resistance of the inner fluid, the internal flow

is slower At the narrowest gap of the constriction, the velocity reaches the maximum for all viscosity ratio while the magnitude of the effect increases due to higher outer fluid velocity at the minimum gap.

However the deformation of droplet while squeezing through constriction shows complex behavior differing in  $x, y, z$ - projection length. At the upstream of constriction, the droplet length in the  $x$ -direction  $L_x$  is highest for the viscosity ratio  $\lambda = 1$ . This maximum deformation is different from the steady-state deformation in that it is in its transient stage. Several other studies have found the maximum of the deformation of a droplet at its transient stage to be the largest at viscosity ratio around  $\lambda = 2$ . Griggs *et al.* reported a droplet moving across a channel towards the centerline has a maximum deformation at  $\lambda = 2$  [18] and Yechun found for a droplet larger than a channel has a maximum deformation at  $\lambda = 2.04$  before it reaches the steady state. However, the reason is unclear and hasn't been describe to date. For the droplets with  $\lambda < 1$ , which can be thought of as bubbles, the decrease of the deformation can be explained with the rate of deformation. The constriction length is not long enough for the droplet to deform fully and since the lower  $\lambda$  droplets travels faster, they have less time to deform. Also the initial slope of the  $L_x$  deformation at the upstream of the constriction for  $\lambda < 1$  is similar but it doesn't reach higher deformation than  $\lambda = 1$  which implies that for droplets with  $\lambda < 1$ , their deformation are limited by the residual time inside the constriction. This discussion can be argued analogous to the growth of the coating film between the droplet-solid surfaces [17]. The discussion by Tsai and Miksis [45] where they reported that for  $Ca = 0.2$  and  $\lambda = 0.001$ , the droplet moves through the constriction too fast for the

thin-film instability to grow and thus the deformation of a droplet surface depends on the velocity of the droplet. The maximum deformation in  $x, y, z$ -coordinates for  $\lambda < 1$  are reached before the constriction.

For droplets with viscosity ratio  $\lambda > 1$ , e.g. a DEGG10 system (a UCON-165 droplet in diethylene-glycol) experimented in a constricted capillary tube by Hemmat and Borhan [20] has viscosity ratio of 2.25, the deformation in  $L_x$  decreases as the viscosity ratio increases. Due to the higher viscosity of the inner fluid and slower fluid flow inside, the droplet needs more time to deform. Thus even though the droplet is move slower in passing the constriction, it is deformed less. The explanation as according to the droplet velocity and it residual time has its proof from the fact that the deformation at the steady state is larger for higher viscosity ratio [18]. At the downstream, we again confirm the discussion by observing that the effect of the droplet velocity for  $\lambda < 1$  on the deformation diminishes while for  $\lambda > 1$ , the effect is valid.

All  $y$ -projection lengths show very small deformation ( $L_y$  deformation difference is less than 3% that of  $L_x$ ). Nevertheless, the  $y$ -projection length of the droplet  $L_y$  shows even more diverse behavior. For  $\lambda > 1$ , the droplet's  $y$ -length reaches a maximum expansion at the narrowest gap of the constriction. As the viscosity ratio is increased the  $y$ -length increases to compensate for the smaller extension in droplet's  $x$ -length. For  $\lambda \leq 1$ , the droplet reaches a minimum just before or at the narrowest constriction gap then extend to a maximum length. Looking at both  $L_x$  and  $L_y$ , we can see that for  $\lambda \leq 1$ , the droplet's maximum or minimum deformation is produced off the center of the constriction whereas for  $\lambda > 1$ , it is always at

$X_c = 0$ . Moreover the in contrast to  $\lambda > 1$ ,  $\lambda \leq 1$  droplets has maximum  $L_x$  at the minimum  $L_y$ . At the downstream of the constriction, the droplet  $y$ -length reaches a minimum, lower as the viscosity ratio decreases. The viscosity ratio  $\lambda < 1$  shows the opposite owing to the droplet velocity as described previously.

The minimum distance between the droplet and the solid  $h_{min}$  is plotted in Figure 4.20(b). The droplet with highest viscosity ratio has the lowest  $h_{min}$  since more viscous droplet deformed less. Figure 4.21 shows the smallest minimum droplet-solid distance we obtained in our computations at capillary number  $Ca = 0.05$  and viscosity ratio  $\lambda = 10$ . The gap decreased as small as 0.027.

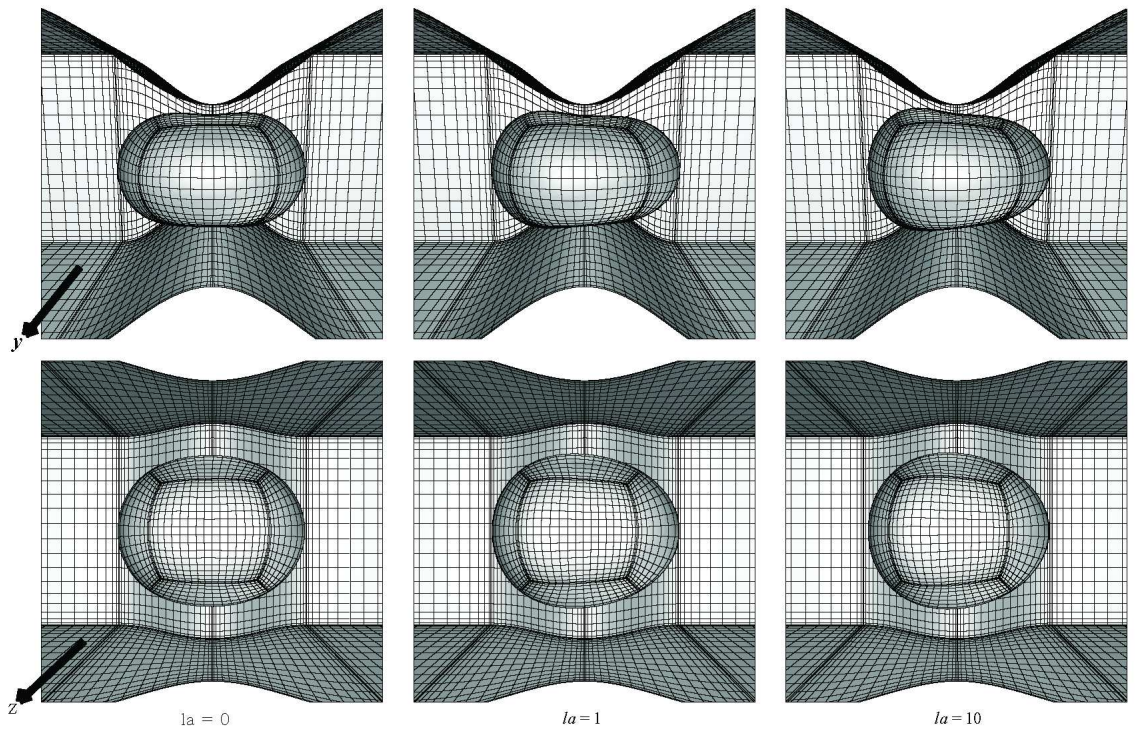


Figure 4.16: Three-dimensional  $y$  and  $z$ -axis shapes of the droplets with  $a = 0.6$ ,  $Ca = 0.1$ ,  $\lambda = 0, 1, 10$ , at  $X_c = 0$ , squeezing through a rectangular full-cosine constriction with 1.0 length and 1.0 minimum gap.

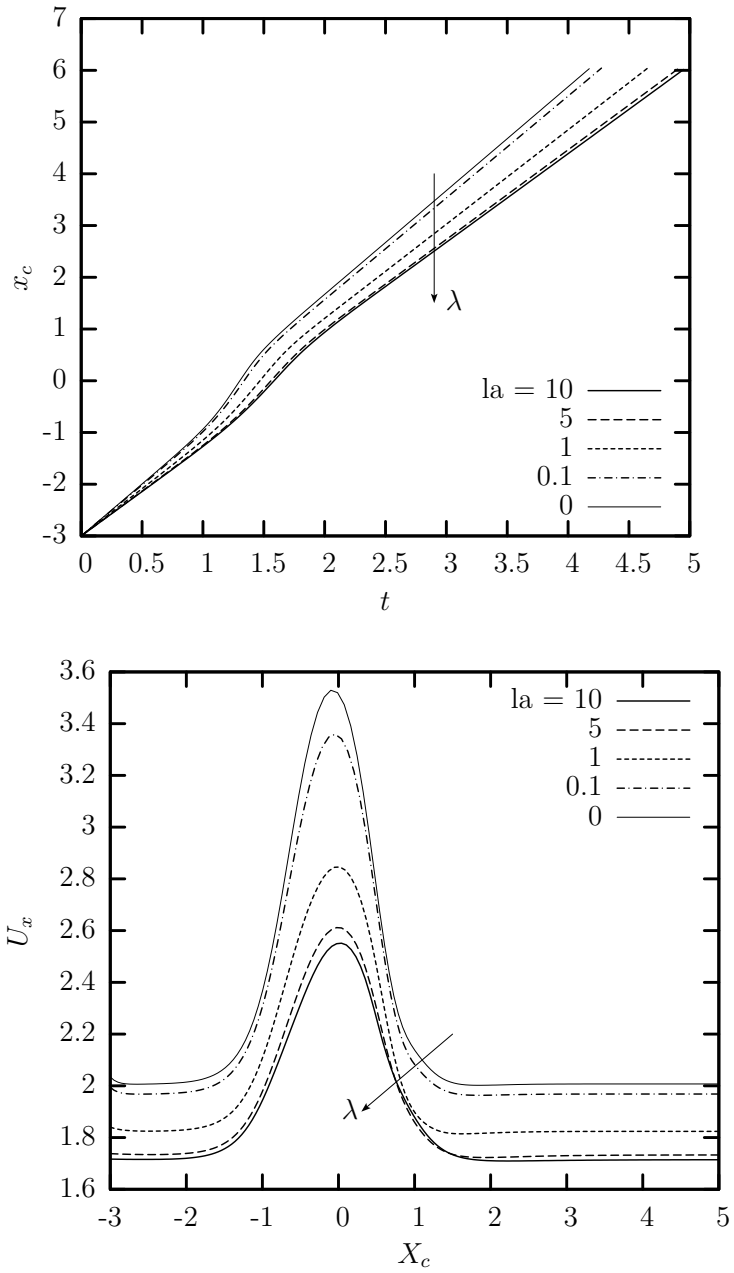


Figure 4.17: (a) Droplet centroid  $X_c$  versus time  $t$  and (b) droplet velocity  $U_x$  versus its centroid  $X_c$  for a droplet with  $a = 0.6$ ,  $Ca = 0.1$  and  $\lambda = 0, 0.1, 1, 5$  and 10 squeezing through a rectangular full-cosine constriction with 1.0 length and 1.0 minimum gap.

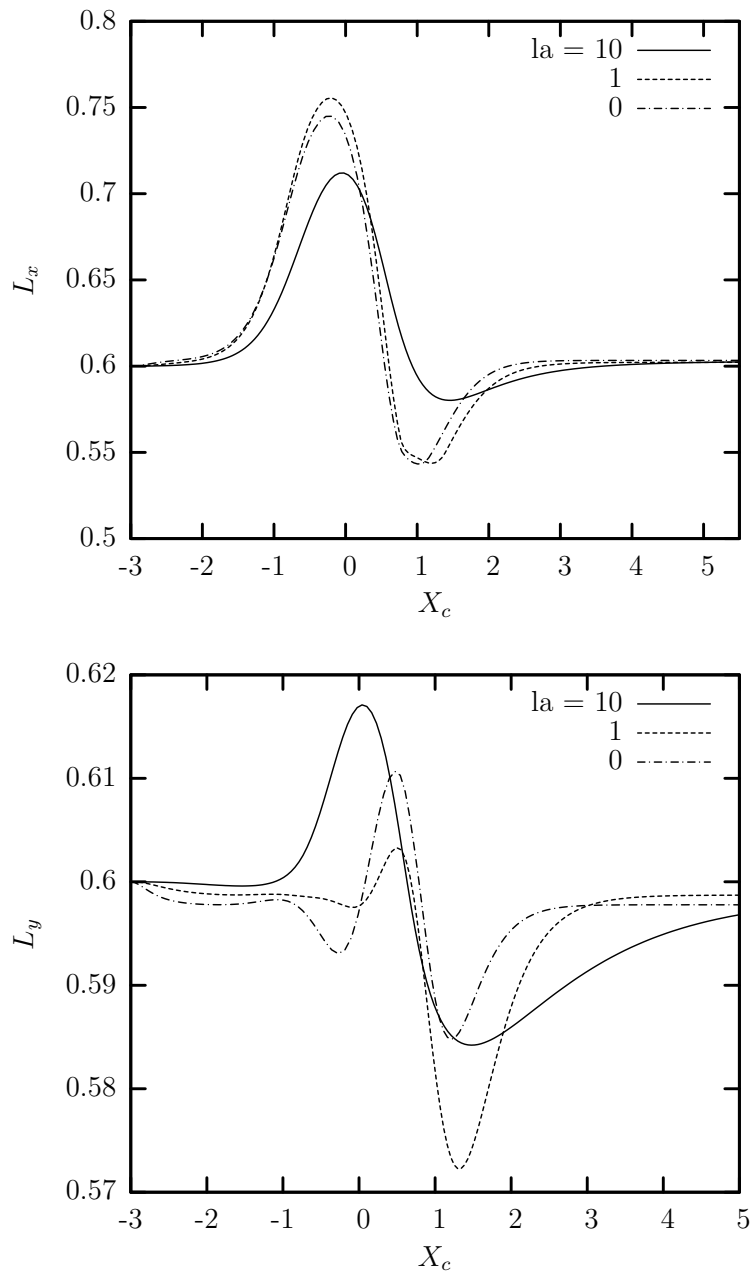


Figure 4.18: (a) Droplet  $x$ -length  $L_x$  and (b)  $y$ -length  $L_y$  versus its centroid  $X_c$  for a droplet with  $a = 0.6$ ,  $Ca = 0.1$  and  $\lambda = 0, 0.1, 1, 5$  and  $10$  squeezing through a rectangular full-cosine constriction with  $1.0$  length and  $1.0$  minimum gap.

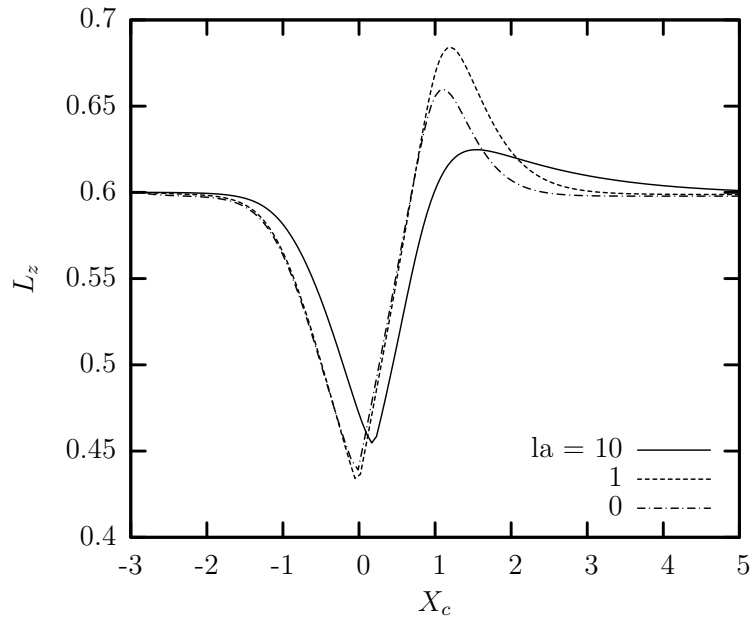


Figure 4.19: Droplet  $z$ -length  $L_z$  versus its centroid  $X_c$  for a droplet with  $a = 0.6$ ,  $Ca = 0.1$  and  $\lambda = 0, 0.1, 1, 5$  and  $10$  squeezing through a rectangular full-cosine constriction with  $1.0$  length and  $1.0$  minimum gap.

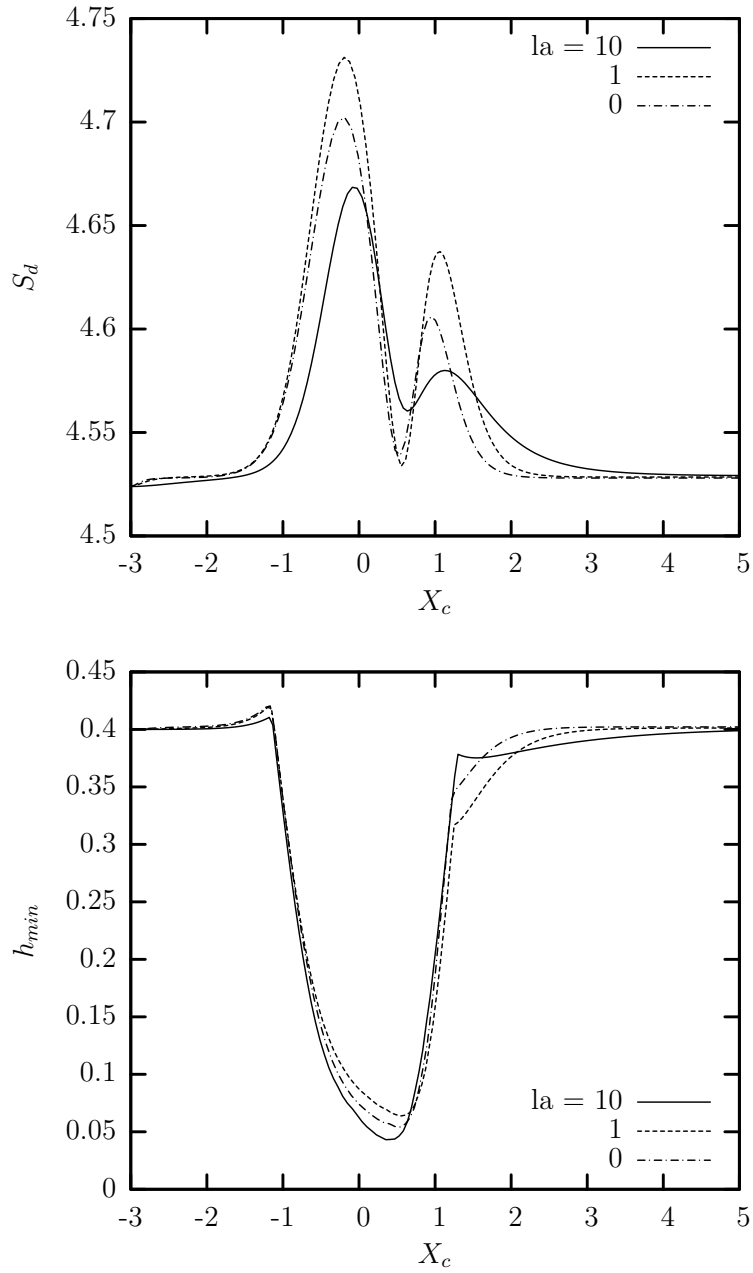


Figure 4.20: (a) Droplet surface area  $S_d$  and (b) droplet-solid minimum distance  $h_{min}$  versus its centroid  $X_c$  for a droplet with  $a = 0.6$ ,  $Ca = 0.1$  and  $\lambda = 0, 0.1, 1, 5$  and 10 squeezing through a rectangular full-cosine constriction with 1.0 length and 1.0 minimum gap.

### 4.3.3 Effects of Constriction Length

Next we consider the effects of the constriction length. All other parameters are fixed, in particular capillary number  $Ca = 0.1$ , viscosity ratio  $\lambda = 5$ , minimum gap 1.0 and droplet size  $a = 0.6$ . The geometries of the different constriction lengths are presented in Figure 4.22.

Investigating the graphs, we can see that the velocity and the deformation is affected by the constriction length due to the actual geometrically length of the constriction. Figure 4.24 shows the velocity of the droplet versus its centroid  $X_c$  and  $X_c$  versus time  $t$ . For longer constriction. the droplet starts to speed up earlier and reaches higher velocity at the center of the bump although the outer fluid velocity is the constant at the minimum constriction gap. Figure 4.25 and Figure 4.26 where the projection lengths in  $x, y, z$ -coordinates are shown deformation increases as the bump length is increased due to the effect of the geometrical shape and the outer fluid velocity thus both the velocity and the shape of the droplet assist each other to make the droplet move faster. On the exit of the constriction, the droplet deformations in all three directions are less for shorter bump length.

Overall, for longer bump length the higher deformation is obtained as shown by the surface area  $S_d$  in Figure 4.27(a). Notice the rate of the droplet lengths  $L_x, L_y, L_z$  deformations and the surface area  $S_d$  change are nearly equal for all bump lengths even though the constriction gradients are different. The rate of deformation shows a limit for a fixed capillary number and viscosity ratio.

The minimum gap between the droplet and the solid  $h_{min}$  decreases as the

constriction length is decreased as shown in Figure 4.27(b) owing to the smaller deformation.

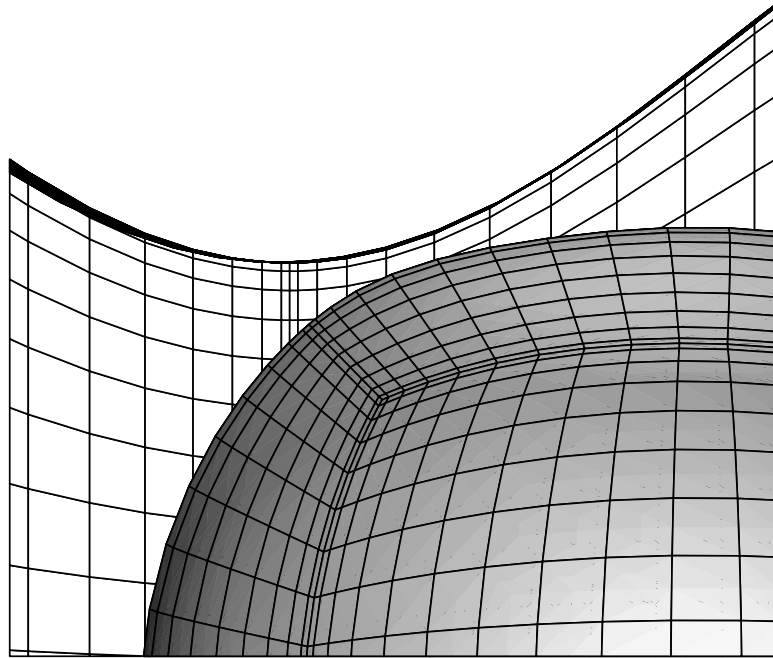


Figure 4.21: Minimum distance between the droplet and the solid  $h_{min} = 0.027$  at  $X_c = 0.46$  for a droplet with  $a = 0.6$ ,  $Ca = 0.05$  and  $\lambda = 10$  squeezing through a rectangular full-cosine constriction with 1.0 length and 1.0 minimum gap.

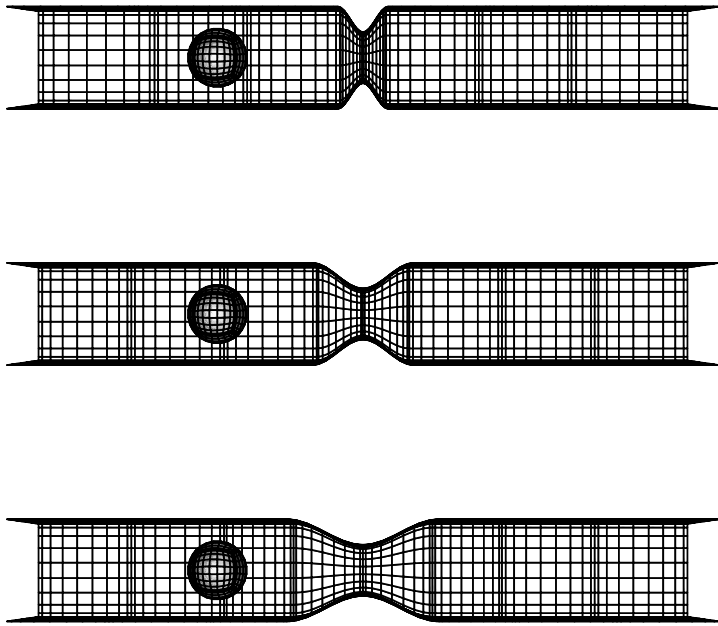


Figure 4.22: Geometries of square channels with a rectangular full-cosine constriction having 1.0, 2.0, 3.0 length and 1.0 minimum gap.

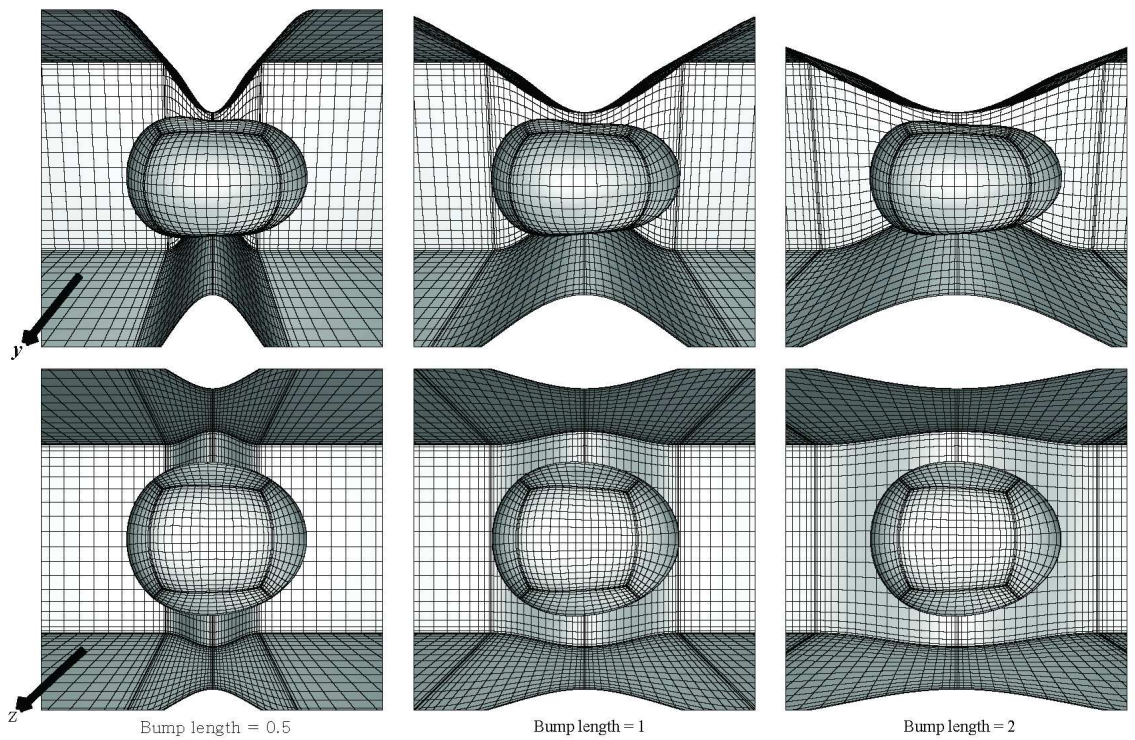


Figure 4.23: Three-dimensional shapes of the droplets with  $a = 0.6$ ,  $Ca = 0.1$ ,  $\lambda = 5$ , at  $X_c = 0$ , squeezing through a rectangular full-cosine constriction with 1.0, 2.0, 3.0 length and 1.0 minimum gap.

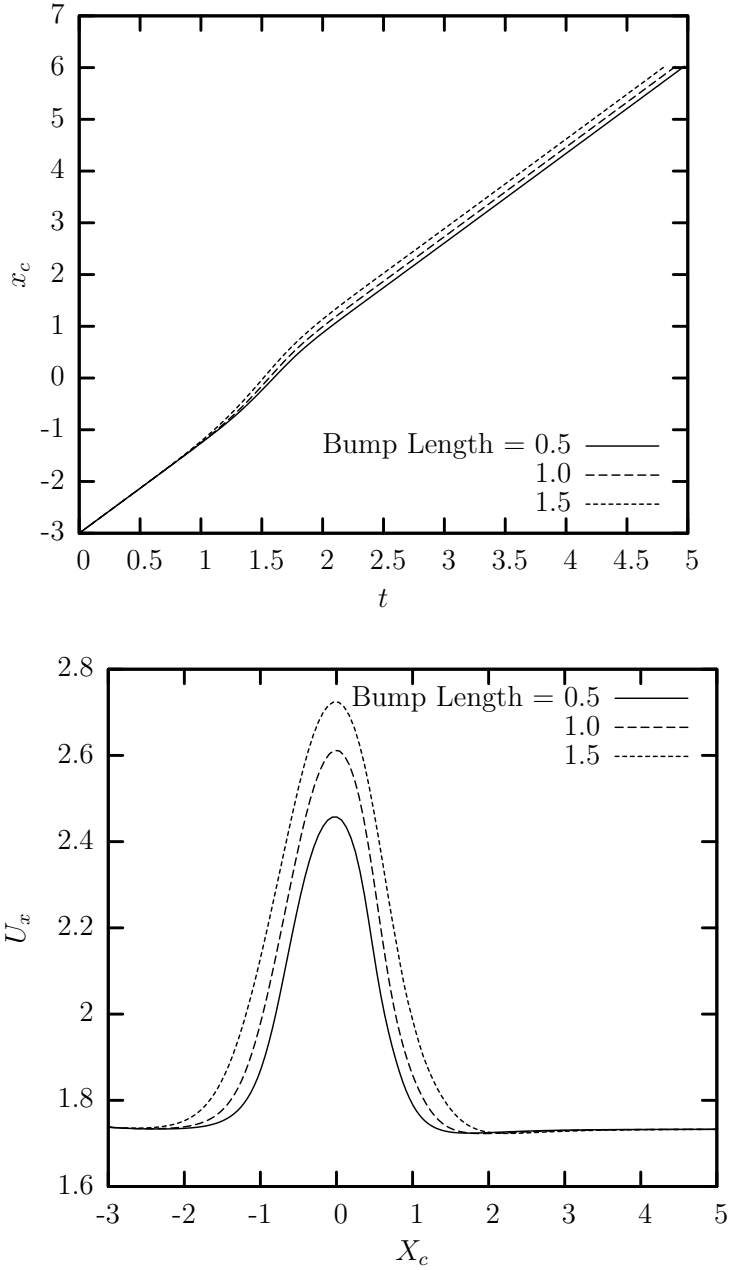


Figure 4.24: (a) Droplet centroid  $X_c$  versus time  $t$  and (b) droplet velocity  $U_x$  versus its centroid  $X_c$  for a droplet with  $a = 0.6$ ,  $Ca = 0.1$  and  $\lambda = 5$  squeezing through a rectangular full-cosine constriction with 1.0, 2.0, 3.0 length and 1.0 minimum gap.

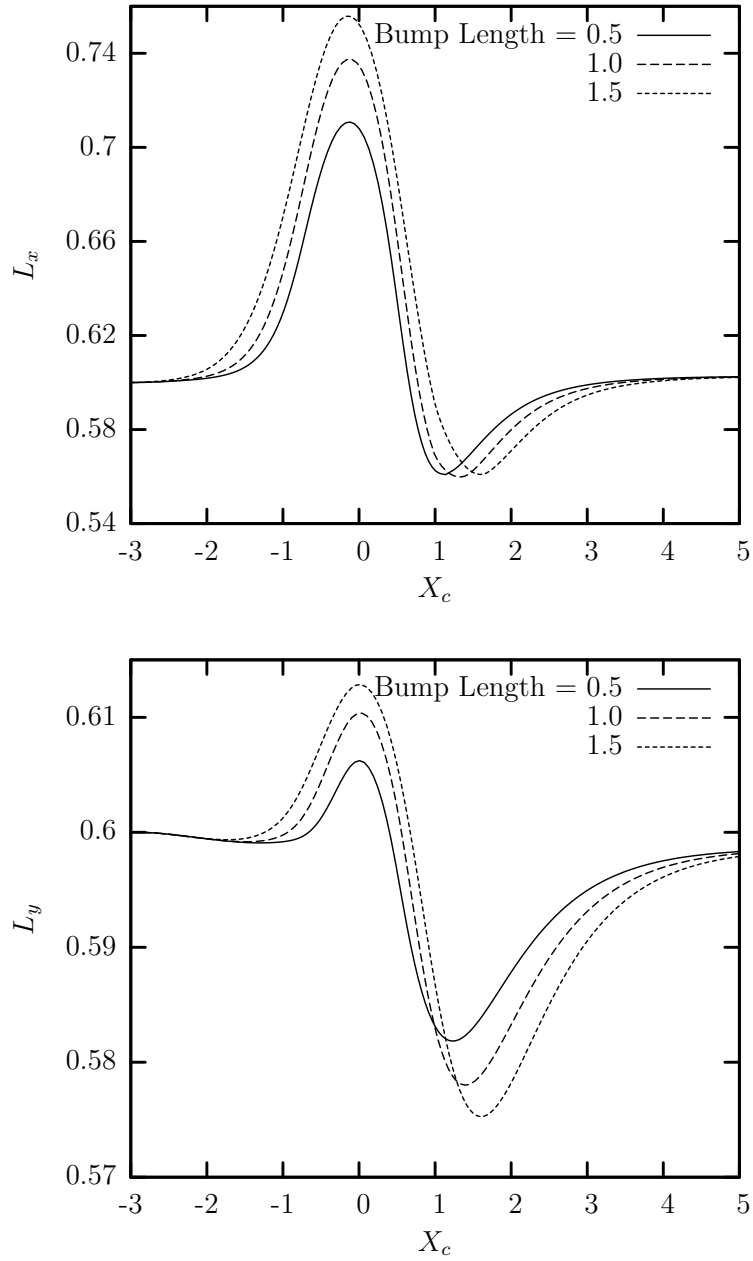


Figure 4.25: (a) Droplet  $x$ -length  $L_x$  and (b)  $y$ -length  $L_y$  versus its centroid  $X_c$  for a droplet with  $a = 0.6$ ,  $Ca = 0.1$  and  $\lambda = 5$  squeezing through a rectangular full-cosine constriction with 1.0, 2.0, 3.0 length and 1.0 minimum gap.

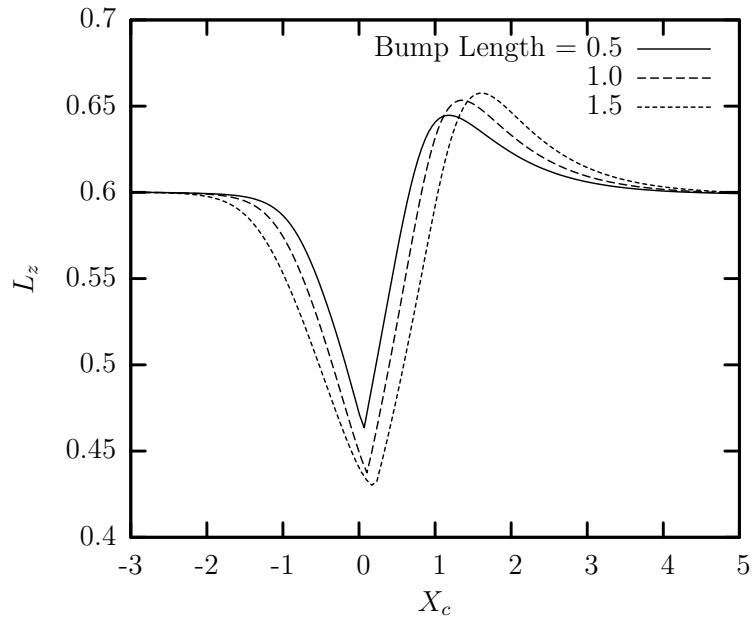


Figure 4.26: Droplet  $z$ -length  $L_z$  versus its centroid  $X_c$  for a droplet with  $a = 0.6$ ,  $Ca = 0.1$  and  $\lambda = 5$  squeezing through a rectangular full-cosine constriction with 1.0, 2.0, 3.0 length and 1.0 minimum gap.

#### 4.3.4 Effects of Constriction Gap

The effects of the constriction gap sizes of 1.4, 1.0 are investigated. Other parameters are set fixed at droplet size  $a = 0.6$ , capillary number  $Ca = 0.1$ , viscosity ratio  $\lambda = 5$  and the constriction length = 1.0. The droplet is smaller than the constriction gap size 1.4 thus the deformation is only induced by the profile of the outer fluid flow. The geometries of the different constriction gap sizes are depicted in Figure 4.28.

Figure 4.29 shows the shapes of the droplet in the constriction with the gap sizes of 1.4 is much less deformed compared to the 1.0 gap size constriction. In Figure 4.30 where the velocity of the droplet versus its centroid  $X_c$  and  $X_c$  versus time  $t$  are shown, the droplet in the channel with the constriction gap sizes of 1.4 is slower.

Figure 4.31, Figure 4.32 and Figure 4.33(a) all show that for the smaller constriction gap size the deformation is higher. A large difference in the minimum gap between the droplet and the solid surface  $S_d$  is shown in Figure 4.33(b).

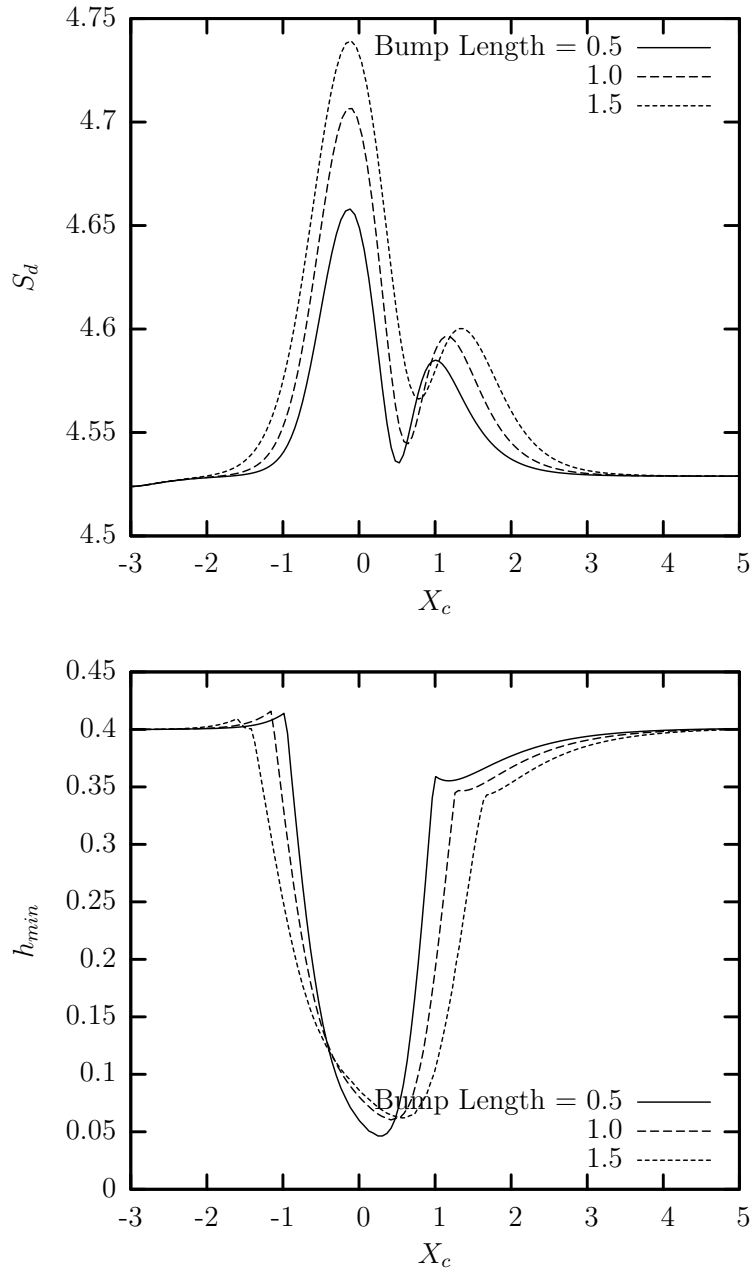


Figure 4.27: (a) Droplet surface area  $S_d$  and (b) droplet-solid minimum distance  $h_{min}$  versus its centroid  $X_c$  for a droplet with  $a = 0.6$ ,  $Ca = 0.1$  and  $\lambda = 5$  squeezing through a rectangular full-cosine constriction with 1.0, 2.0, 3.0 length and 1.0 minimum gap.

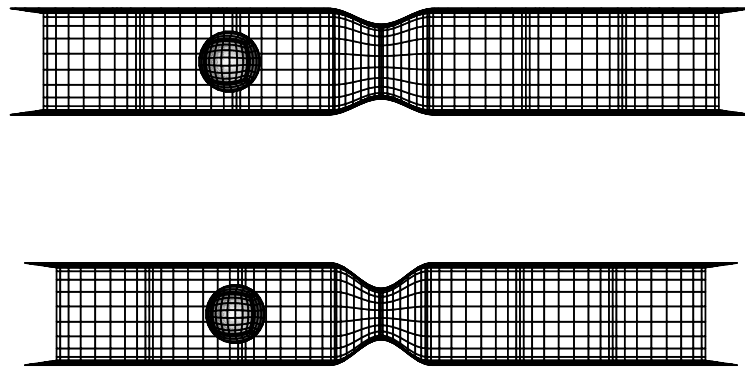


Figure 4.28: Geometries of square channels with a rectangular full-cosine constriction having 1.0 length and 1.4, 1.0 minimum gap.

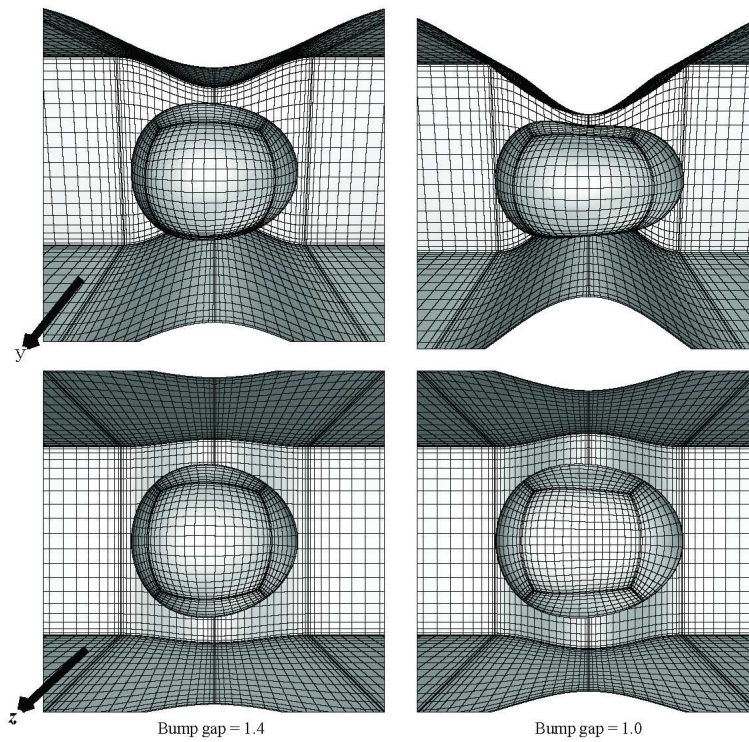


Figure 4.29: Three-dimensional shapes of the droplets with  $a = 0.6$ ,  $Ca = 0.1$ ,  $\lambda = 5$ , at  $X_c = 0$ , squeezing through a rectangular full-cosine constriction with 1.0 length and 1.4, 1.0 minimum gap.

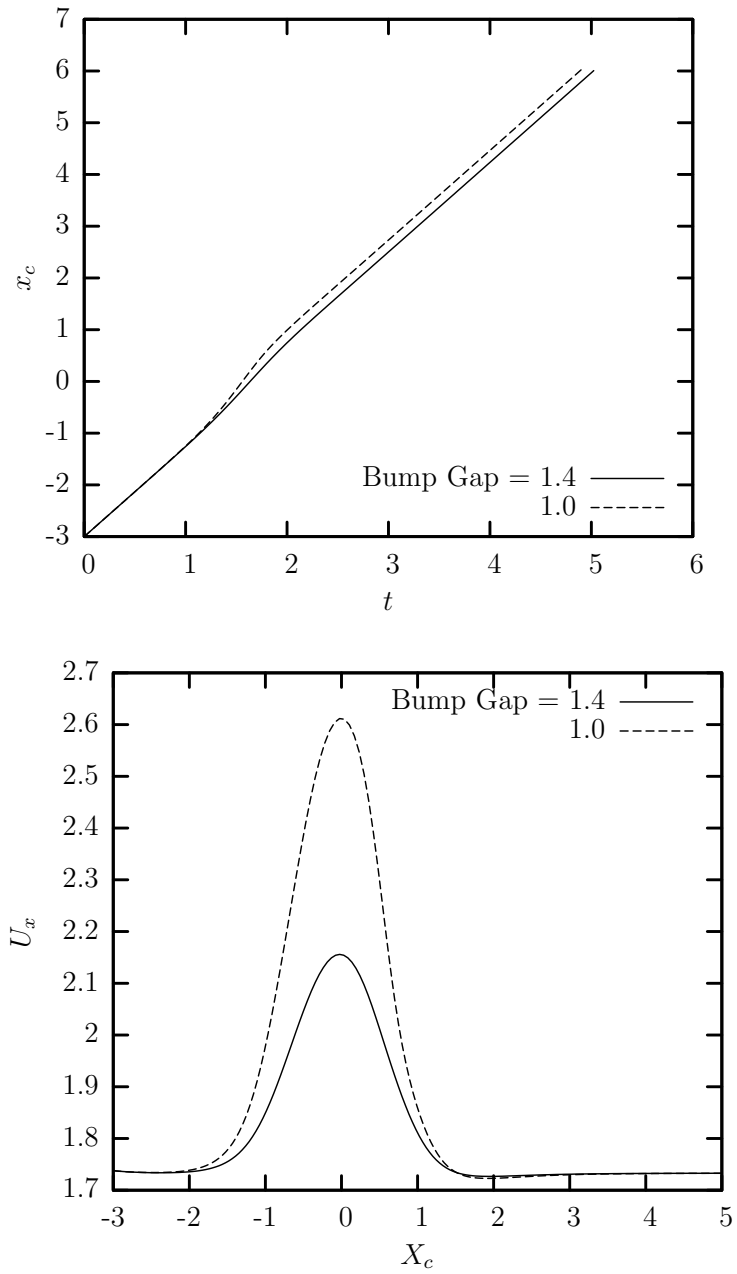


Figure 4.30: (a) Droplet centroid  $X_c$  versus time  $t$  and (b) droplet velocity  $U_x$  versus its centroid  $X_c$  for a droplet with  $a = 0.6$ ,  $Ca = 0.1$  and  $\lambda = 5$  squeezing through a rectangular full-cosine constriction with 1.0 length and 1.4, 1.0 minimum gap.

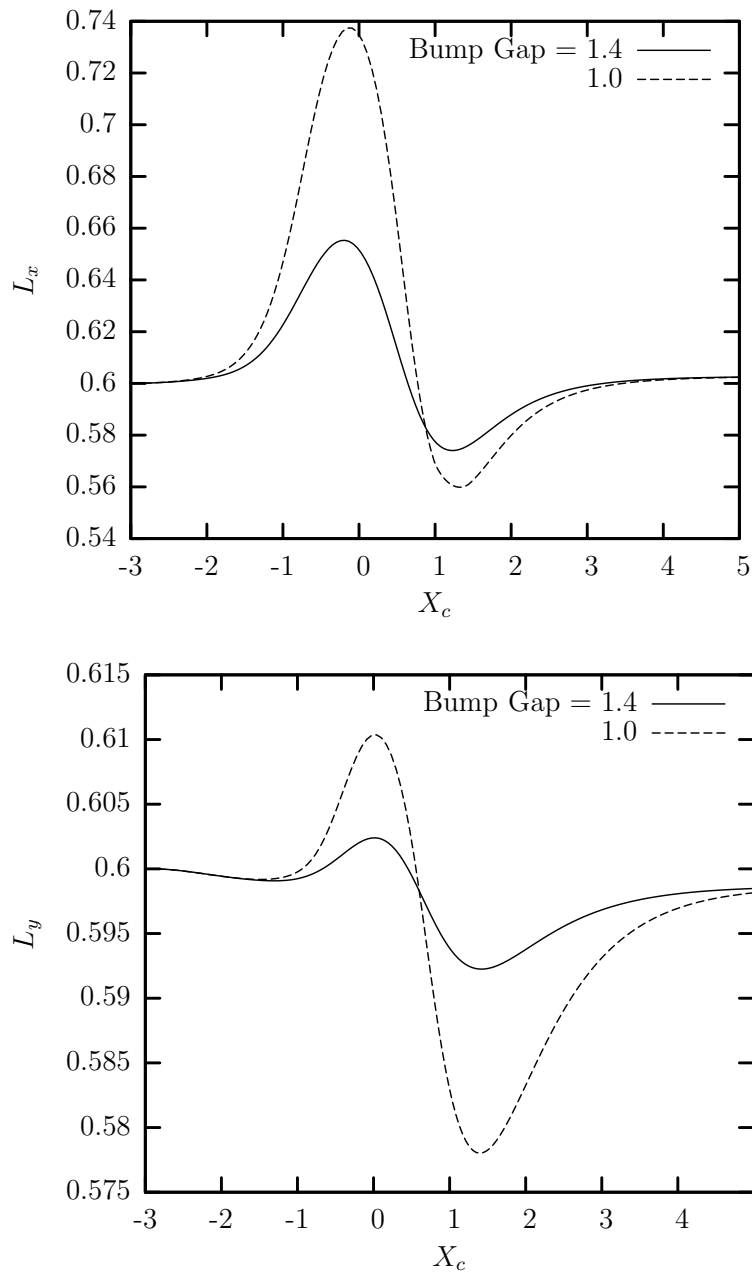


Figure 4.31: (a) Droplet  $x$ -length  $L_x$  and (b)  $y$ -length  $L_y$  versus its centroid  $X_c$  for a droplet with  $a = 0.6$ ,  $Ca = 0.1$  and  $\lambda = 5$  squeezing through a rectangular full-cosine constriction with 1.0 length and 1.4, 1.0 minimum gap.

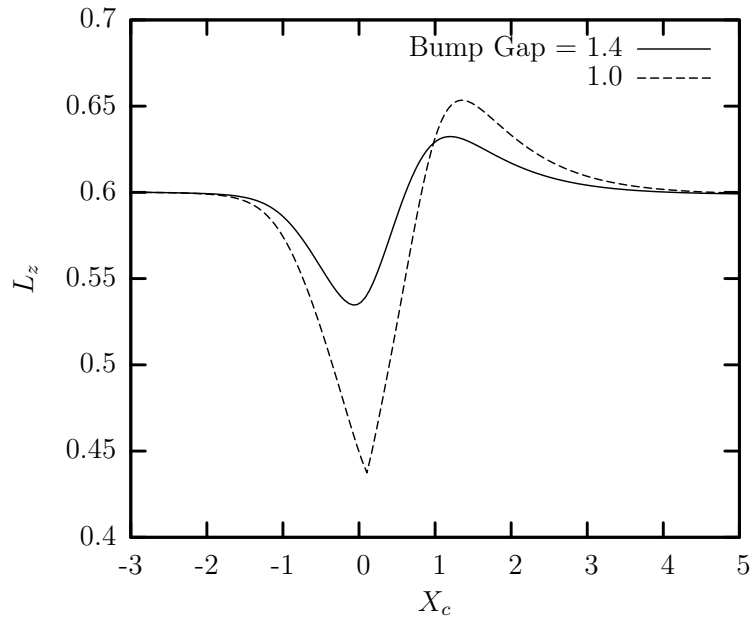


Figure 4.32: Droplet  $z$ -length  $L_z$  versus its centroid  $X_c$  for a droplet with  $a = 0.6$ ,  $Ca = 0.1$  and  $\lambda = 5$  squeezing through a rectangular full-cosine constriction with 1.0 length and 1.4, 1.0 minimum gap.

In the range of the parameters studied in this thesis, our results show no sign of snap-off. The droplet doesn't produce any threads inside the constriction which is a sign for snapping-off. The rectangular constriction having no "neck" by which we mean constriction in both  $y, z$ -axis, it is much harder for the droplet to break into daughter droplets and the mechanism of the droplet snap-off should be different.

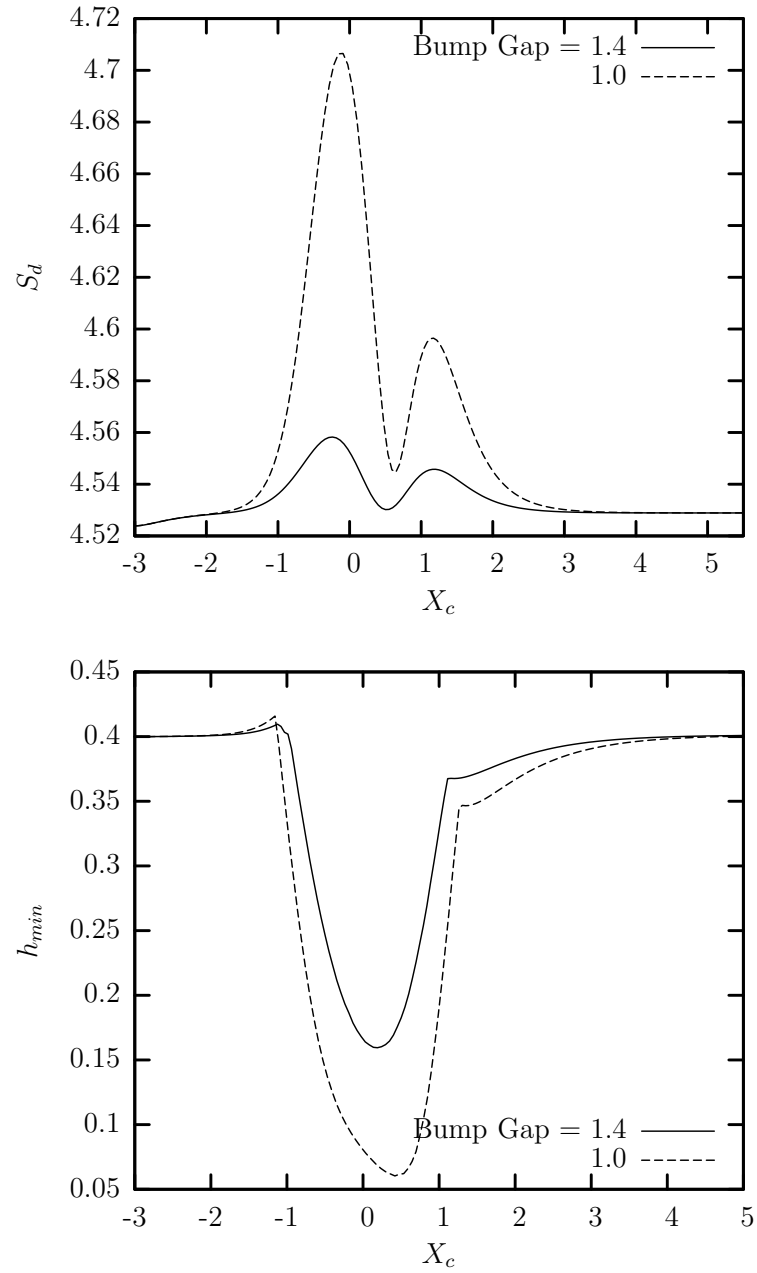


Figure 4.33: (a) Droplet surface area  $S_d$  and (b) droplet-solid minimum distance  $h_{min}$  versus its centroid  $X_c$  for a droplet with  $a = 0.6$ ,  $Ca = 0.1$  and  $\lambda = 5$  squeezing through a rectangular full-cosine constriction with 1.0 length and 1.4, 1.0 minimum gap.

## 4.4 Conclusion

We examined the squeezing motion of a single droplet in a square cross-sectional microfluidic channel with a rectangular constriction filled with another immiscible fluid. We started by investigating the differences between a square and a rectangular constriction in a square microchannel. Then we considered the influences of the capillary number, fluids' viscosities and the geometric size on the droplet interfacial shape, droplet velocity and the minimum gap between the droplet and the solid wall.

The capillary number and the viscosity ratio we investigated have some similar behavior on the droplet squeezing through constriction compared to that of the previous studies on an axisymmetric tube. As we increased the capillary number we found higher deformation and thicker fluid between the droplet and solid surface. As we increased the viscosity ratio, the droplet acted as a more rigid droplet and deformed slower. However, due to the non-symmetric geometry of our constriction different dynamics and motion of the droplet was also identified. In particular, owing to the unconstricted  $y$ -axis, the droplet formed a flat disk shape and the overall deformation of the droplet was smaller. For lower capillary numbers and larger viscosity ratios, the droplet's  $y$ -length deformed more but only in a very small magnitude and for all runs it stayed within 3% of its original length.

At least in the range of parameters studied here, no sign of snap-off of the droplet was found since owing to the rectangular constriction, the droplet does not show a "neck". In the case of a smaller rectangular gap, the mechanism of the droplet

snap-off, if any, is expected to be different compared to a axisymmetric constriction. This would be of a great interest in our further study since it can provide a guidance in the designing of microfluidic devices where rectangular channels are commonly used for emulsion production or sorting.

## Bibliography

- [1] A. Arriola, G. P. Willhite and D. Greenet, Trapping of oil drops in a non-circular pore throat and mobilization upon contact with a surfactant. *Soc. Petrol. Eeng. J.* **23**(1), 99–114 (1983).
- [2] F. P. Bretherton, The motion of long bubbles in tubes. *J. Fluid Mech.* **10**(2), 166–188 (1961).
- [3] E. Chmela, M. T. Blom, J. G. E. Gardeniers, A. Berg and R. Tijssen, A pressure driven injection system for an ultra-flat chromatographic microchannel. *Lab Chip* **2**(4), 235–241 (2002).
- [4] R. H. Davis and A. Z. Zinchenko, Motion of deformable drops through granular media and other confined geometries. *J. Colloid. Interf Sci.* **334**(2), 113–123 (2009).
- [5] P. Dimitrakopoulos and J. J. L. Higdon, Displacement of fluid droplets from solid surfaces in low-Reynolds-number shear flows. *J. Fluid Mech.* **336**, 351–378 (1997).
- [6] P. Dimitrakopoulos and J. J. L. Higdon, On the displacement of three-dimensional fluid droplets from solid surface in low-Reynolds-number shear flows. *J. Fluid Mech.* **377**, 189–222 (1998).
- [7] P. Dimitrakopoulos and J. J. L. Higdon, On the gravitational displacement of three-dimensional fluid droplets from inclined solid surfaces. *J. Fluid Mech.* **395**, 181–209 (1999).

- [8] P. Dimitrakopoulos and J. J. L. Higdon, On the displacement of three-dimensional fluid droplets adhering to a plane wall in viscous pressure-driven flows. *J. Fluid Mech.* **435**, 327–350 (2001).
- [9] P. Dimitrakopoulos and J. J. L. Higdon, On the displacement of fluid bridges from solid surfaces in viscous pressure-driven flows. *Phys. Fluids* **15**(10), 3255–3258 (2003).
- [10] P. Dimitrakopoulos, Deformation of a droplet adhering to a solid surface in shear flow: onset of interfacial sliding. *J. Fluid Mech.* **580**, 451-466 (2007).
- [11] P. Dimitrakopoulos, Interfacial dynamics in Stokes flow via a three-dimensional fully-implicit interfacial spectral boundary element algorithm. *J. Comput. Phys.* **225**(1), 408-426 (2007).
- [12] P. Dimitrakopoulos and J. Wang, A spectral boundary element algorithm for interfacial dynamics in two-dimensional Stokes flow based on Hermitian interfacial smoothing. *Eng. Anal. Bound. Elem.* **31**(7), 646-656 (2007).
- [13] P. Dimitrakopoulos, Gravitational effects on the deformation of a droplet adhering to a horizontal solid surface in shear flow. *Phys. Fluids* **19**(12), 122105 (2007).
- [14] W. R. Dodson and P. Dimitrakopoulos, Spindles, cusps, and bifurcation for capsules in Stokes flow. *Phys. Rev. Lett.* **101**(20), 208102 (2008).
- [15] W. R. Dodson and P. Dimitrakopoulos, Dynamics of strain-hardening and strain-softening capsules in strong planar extensional flows via an interfacial spec-

- tral boundary element algorithm for elastic membranes. *J. Fluid. Mech.* **641**, 263–296 (2009).
- [16] P. A. Gauglitz, C. M. St. Laurent, C. J. Radke, An experimental investigation of gas-bubble breakup in constricted square capillaries. *SPE CA Meeting*, (1987).
- [17] P. A. Gauglitz, C. J. Radke, The dynamics of liquid film breakup in constricted cylindrical capillaries. *J. Colloid Int. Sci.*, **134** 14–40 (1990).
- [18] A. J. Griggs, A. Z. Zinchenko and R. H. Davis, Low-Reynolds-number motion of a deformable drop between two parallel plane walls. *Int. J. Multiphas. Flow* **33**(2), 182–206 (2007).
- [19] C. Han and K. Funatsu, An experimental study of droplet deformation and breakup in pressure-driven flows through converging and uniform channels. *J. Rheol.* **22**(2), 113–133 (1978).
- [20] Hemmat M, Borhan A, Buoyancy-driven motion of drops and bubbles in a periodically constricted capillary. *Chem. Eng. Comm.* **150**, 363–384 (1996).
- [21] B. P. Ho and L. G. Leal, Creeping motion of liquid drops through a circular tube of comparable diameter. *J. Fluid Mech.* **71**, 361– (1975).
- [22] A. Huebner, S. Sharma, M. Srisa-Art, F. Hollfelder, J. B. Edel and A. J. Demello Microdroplets: A sea of applications. *Lab Chip* **8**(8), 1244–1254 (2008).

- [23] P. J. A. Janssen and P. D. Anderson, A boundary-integral model for drop deformation between two parallel plates with non-unit viscosity ratio drops. *J. Comp. Phys.* **227**(22), 435–450 (2008).
- [24] M. J. Jensen, H. A. Stone and H. Bruus, A numerical study of two-phase Stokes flow in an axisymmetric flow-focusing device. *Phys. Fluid* **18**, 435–450 (2006).
- [25] N. Korin, A. Bransky, M. Khoury, U. Dinnar and S. Levenberg, Design of well and groove microchannel bioreactors for cell culture. *Biotechnol. Bioeng.* **102**(4), 1222–1230 (2009).
- [26] A. Leyrat-Maurin and D. Barthes-Biesel, Motion of a deformable capsule through a hyperbolic constriction. *J. Fluid Mech.* **279**, 135–163 (1994).
- [27] M. J. Martinez and K. S. Udell, Axisymmetric creeping motion of drops through a periodically constricted tube. *AIP Conf. Proc.* **197**, 222–234 (1988).
- [28] M. J. Martinez and K. S. Udell, Axisymmetric creeping motion of drops through circular tubes. *J. Fluid Mech.* **210**, 565–591 (1990).
- [29] M. Muradoglu and S. Gokaltun Implicit multigrid computations of buoyant drops through sinusoidal constrictions. *J. App. Mech.* **71**(), 857–865 (2004).
- [30] W. L. Olbricht and L. G. Leal, The Creeping Motion of Immiscible Drops through a Converging Diverging Tube. *J. Fluid Mech.* **134**, 329–355 (1983).
- [31] W. L. Olbricht, Pore-scale prototypes of multiphase flow in porous media. *Annu. Rev. Fluid Mech.* **28**, 187–213 (1996).

- [32] U. Olgac, A. D. Kayaalp and M. Muradoglu, Buoyancy-driven motion and breakup of viscous drops in constricted capillaries. *Int. J. Multiphas. Flow* **32**, 1055–1071 (2006).
- [33] C. Pozrikidis, *Boundary Integral and Singularity Methods for Linearized Viscous Flow*. Cambridge University Press, Cambridge (1999).
- [34] C. Pozrikidis, A spectral-element method for particulate Stokes flow. *J. Comput. Phys.*, **156**, 360 (1999).
- [35] C. Pozrikidis, Effect of pressure gradient on viscous shear flow past an axisymmetric depression or protuberance on a plane wall. *Comp. Fluids* **29**, 617–637 (2000).
- [36] J. Ratulowski and H. C. Chang, Snap off at strong constrictions - Effect of pore geometry. *ACS Sym. Ser.* **373**, 282–294 (1988).
- [37] G. J. Roof, Snap-off of oil droplets in water-wet pores. *Soc. Petrol. Eng. J.* **10**(1), 85–90 (1970).
- [38] Y. Song, J. Hormes and C. Kumar, Microfluidic synthesis of nanomaterials. *Small* **4**(6), 698–711 (2008).
- [39] M. Shapira and S. Haber, Low Reynolds-number motion of a droplet between 2 parallel plates. *Int. J. Multiphas. Flow* **14**(4), 483–506 (1988).
- [40] H. Song, J. D. Tice and R. F. Ismagilov, A microfluidic system for controlling reaction networks in time. *Angew. Chem. Int. Edit.* **42**(7), 768–772 (2003).

- [41] M. E. Staben, A. Z. Zinchenko and R. H. Davis, Motion of a particle between two parallel plane walls in low-Reynolds-number Poiseuille flow. *Phys. Fluids* **15**(6), 1711-1733 (2003).
- [42] M. L. J. Steegmans, K. G. P. H. Schroen and R. M. Boom Characterization of Emulsification at Flat Microchannel Y Junctions. *Langmuir* **25**(6), 3396-3401 (2009).
- [43] Y. C. Tan, J. S. Fisher, A. I. Lee, V. Cristini and A. P. Lee, Design of microfluidic channel geometries for the control of droplet volume, chemical concentration, and sorting. *Lab Chip* **4**(4), 292-298 (2004).
- [44] S. Thomas, Enhanced oil recovery - An overview. *Oil Gas Sci. Technol.* **63**(1), 9-19 (2008).
- [45] T. M. Tsai and M. J. Miksis, Dynamics of a Drop in a Constricted Capillary-Tube. *J. Fluid Mech.* **274**, 197-217 (1994).
- [46] A. Vananroye, P. Van Puyvelde and P. Moldenaers, Structure development in confined polymer blends: Steady-state shear flow and relaxation. *Langmuir* **22**, 2273-2280 (2006).
- [47] A. Vananroye, P. Van Puyvelde and P. Moldenaers, Effect of confinement on droplet breakup in sheared emulsions. *Langmuir* **22**, 3972-3974 (2006).
- [48] Y. Wang and P. Dimitrakopoulos, Normal force exerted on vascular endothelial cells. *Phys. Rev. Lett.* **96**, 028106 (2006).

- [49] Y. Wang and P. Dimitrakopoulos, Nature of the hemodynamic forces exerted on vascular endothelial cells or leukocytes adhering to the surface of blood vessels. *Phys. Fluids* **18**(8), 087107 (2006).
- [50] Y. Wang and P. Dimitrakopoulos, A three-dimensional spectral boundary element algorithm for interfacial dynamics in Stokes flow. *Phys. Fluids* **18**(8), 082106 (2006).
- [51] W. R. Rossen, Snap-off in constricted tubes and porous media. *Colloid Surface A* **166**, 101–107 (2000).
- [52] C. Yih, *Fluid Mechanics - A concise introduction to the theory*. West River Press, University of Michigan (1979).
- [53] G. K. Youngren and A. Acrivos, Shape of a gas bubble in a viscous extensional flow. *J. Fluid Mech.* **76**, 433–442 (1976).
- [54] A. Z. Zinchenko and R. H. Davis, A boundary-integral study of a drop squeezing through interparticle constrictions. *J. Fluid Mech.* **564**, 227–266 (2006).

## Vita

Moon Soo Lee was born on May 23rd, 1980, in Seoul, South Korea. He attended the Hanyoung Foreign Language High School from March 1996 to December 1997. He entered the Yonsei University, the Department of Chemical Engineering in Seoul, South Korea in March 1999. After two years of military service in the Korean Army from April 2002 to June 2005, he graduated in February 2007 and received his Bachelor of Science degree in Chemical Engineering. He worked at the Hyundai Engineering company as a process engineer between January 2007 and May in 2007 then he moved to the US. In September 2007, he was enrolled at the graduate program of the Department of Chemical and Biomolecular Engineering at the University of Maryland at College Park. He joined the Bio Fluid Dynamics Laboratory and conducted research in the area of computational fluid dynamics under the guidance of Professor Panagiotis Dimitrakopoulos. His graduate work involved the study of the interfacial dynamics of a droplet in a microchannel. In January 2010, he received his Master of Science degree in Chemical Engineering with thesis titled “Computational studies of droplet motion and deformation in a microfluidic channel with a constriction”.